Published in final edited form as:

*Cancer Discov*. 2020 February ; 10(2): 270–287. doi:10.1158/2159-8290.CD-19-0780.

# *In vivo* epigenetic CRISPR screen identifies *Asf1a* as an immunotherapeutic target in *Kras*-mutant lung adenocarcinoma

**Fei Li**[1,2], **Qingyuan Huang**[1,2], **Troy A. Luster**[3], **Hai Hu**[1], **Hua Zhang**[1,2], **Wai-Lung Ng**[4,10,11], **Alireza Khodadadi-Jamayran**[5], **Wei Wang**[6], **Ting Chen**[1,2], **Jiehui Deng**[1,2], **Michela Ranieri**[1], **Zhaoyuan Fang**[7], **Val Pyon**[1], **Catríona M. Dowling**[1], **Ece Bagdatlioglu**[1], **Christina Almonte**[1], **Kristen Labbe**[1], **Heather Silver**[1], **Alexandra R. Rabin**[1], **Kandarp Jani**[1,2], **Aristotelis Tsirigos**[5,8], **Thales Papagiannakopoulos**[8], **Peter S. Hammerman**[2], **Vamsidhar Velcheti**[1], **Gordon J. Freeman**[2,9], **Jun Qi**[4,10], **George Miller**[6], **Kwok-Kin Wong**[1,2,3,9]

[1]Division of Hematology & Medical Oncology, Laura and Isaac Perlmutter Cancer Center, New York University Langone Medical Center, New York, New York.

[2]Department of Medical Oncology, Dana-Farber Cancer Institute, Boston, Massachusetts.

[3]Belfer Center for Applied Cancer Science, Dana-Farber Cancer Institute, Boston, Massachusetts.

[4]Department of Cancer Biology, Dana-Farber Cancer Institute, Boston, Massachusetts.

[5]Applied Bioinformatics Laboratories and Genome Technology Center, Division of Advanced Research Technologies, New York University Langone Medical Center, New York, New York.

[6]S. Arthur Localio Laboratory, Department of Surgery, New York University School of Medicine, New York, New York.

[7]State Key Laboratory of Cell Biology, Innovation Center for Cell Signaling Network, CAS Center for Excellence in Molecular Cell Science, Shanghai Institute of Biochemistry and Cell Biology, Chinese Academy of Sciences, University of Chinese Academy of Sciences, Shanghai.

[8]Department of Pathology, New York University School of Medicine, 550 First Avenue, New York, New York.

**Corresponding Author:** Kwok-Kin Wong, New York University Langone Medical Center, 550 1st Avenue, Smilow 1011, New York, NY 10016. Phone: 212-263-9203; Fax: 617-632-7839; kwok-kin.wong@nyulangone.org, Contact telephone: +1-212-263-9203.

AUTHOR CONTRIBUTIONS

F.L., T.A.L., and K.K.W. conceived the project and designed the research. F.L. and T.A.L. constructed the epigenetic-focused sgRNA library. F.L., Q.H., and H.H. performed CRISPR screen and candidate validation. F.L., Q.H., and H.H. performed treatment studies. F.L., H.H. and M.R. performed further functional and mechanistic studies. W.L.N., A.J., Z.F., A.T. and J.Q. performed bioinformatics data analysis. H.Z., W.W., T.C., J.D., V.P., C.A., E.B., C.A., K.L., H.S., A.R., K.J. and G.J.F. provided technical and material support. T.P., P.S.H, V.V., G.J.F., J.Q. and G.M. provided many constructive suggestions. F.L., Q.H., T.A.L., H.Z., W.L.N., C.M.D., A.R., T.P., P.S.H., V.V., G.J.F., J.Q., G.M. and K.K.W. wrote and revised the manuscript.

No potential conflicts of interest were disclosed by the other authors.

DISCLOSURES

K.K.W. is a founder and equity holder of G1 Therapeutics, and he has consulting/sponsored research agreements with the following: (consulting & sponsored research) AstraZeneca, Janssen, Pfizer, Novartis, Merck, Ono, and Array; (sponsored research only) MedImmune, Takeda, TargImmune, and BMS.

K.K.W., F.L., Q.H., and H.H. have ownership interest in a patent application.

G.J.F has patents/pending royalties on the PD-1 pathway from Roche, Merck, Bristol-Myers-Squibb, EMD-Serono, Boehringer-Ingelheim, AstraZeneca, Dako and Novartis. G.J.F has served on advisory boards for Novartis, Roche, Bristol-Myers Squibb, Xios, and OrigiMed.

[9]Department of Medicine, Brigham and Women's Hospital, Harvard Medical School, Boston, Massachusetts.

[10]Department of Medicine, Harvard Medical School, Boston, Massachusetts.

[11]School of Pharmacy, Faculty of Medicine, The Chinese University of Hong Kong, Sha Tin, Hong Kong SAR.

## Abstract

Despite substantial progress in lung cancer immunotherapy, the overall response rate in *KRAS*-mutant lung adenocarcinoma (ADC) patients remains low. Combining standard immunotherapy with adjuvant approaches that enhance adaptive immune responses—such as epigenetic modulation of anti-tumor immunity—is therefore an attractive strategy. To identify epigenetic regulators of tumor immunity, we constructed an epigenetic-focused sgRNA library, and performed an *in vivo* CRISPR screen in a $Kras^{G12D}/P53^{-/-}$ (KP) lung ADC model. Our data showed that loss of the histone chaperone *Asf1a* in tumor cells sensitizes tumors to anti-PD-1 treatment. Mechanistic studies revealed that tumor cell-intrinsic *Asf1a* deficiency induced immunogenic macrophage differentiation in the tumor microenvironment by upregulating GM-CSF expression and potentiated T cell activation in combination with anti-PD-1. Our results provide rationale for a novel combination therapy consisting of ASF1A inhibition and anti-PD-1 immunotherapy.

### Keywords

epigenome; CRISPR screen; *Asf1a*; immunotherapy; PD-1; lung adenocarcinoma

## INTRODUCTION

Lung adenocarcinoma (ADC) is a leading cause of cancer-related mortality worldwide (1). *KRAS* (32%) and *EGFR* (11%) mutations are major oncogenic drivers in lung ADC (2). Molecular targeted therapy is a promising therapeutic modality for lung ADC patients compared to conventional chemotherapy or radiotherapy. Lung ADC patients with *EGFR* mutations can benefit from EGFR tyrosine kinase inhibitors (TKI) (3–5). Despite the development of allele-specific KRASG12C inhibitors (6–8), KRAS remains an elusive target for direct inhibitors (9), highlighting an urgent need to develop new therapeutic strategies for *KRAS*-mutant patients. In this regard, immunotherapy has provided additional treatment options for cancer patients. Blockade of inhibitory immune-checkpoint receptors such as programmed cell death protein 1 (PD-1) and cytotoxic T-lymphocyte-associated protein 4 (CTLA-4) have achieved clinical success in multiple cancers including lung ADC (10). However, the immunotherapeutic response rate in *KRAS*-mutant patients remains unsatisfactory (11). Combining immunotherapy with adjuvant approaches that enhance adaptive immune responses is therefore a potential strategy (12).

Epigenetic genes play important roles in cancer biology (13), and accumulating evidence indicates that epigenetic factors are involved in modulating the tumor immune microenvironment (TME) and regulating the anti-tumor immune response. For example,

DNA methyltransferases (DNMTs), histone deacetylases (HDACs), enhancer of zeste homolog 2 (EZH2), bromodomain containing 4 (BRD4), and lysine-specific histone demethylase 1A (LSD1) play important roles in cancer biology and can modulate anti-tumor immunity (14–17). However, the utility of epigenetic regulators in potentiating cancer immunotherapy remains under-explored. CRISPR-Cas9 has expanded the use of functional genetic screens for rapid target discovery in immunotherapy (18–20). Specifically, co-culture systems have been used to screen for factors regulating interactions between cancer cells and immune cells (19,20). However, these *in vitro* screen designs do not faithfully capture the complex interactions that occur within the endogenous tumor microenvironment. *In vivo* models can be a more relevant setting to screen for tumor-immune interactions, but are challenging considering the technical difficulty in maintaining sgRNA representation *in vivo* (21). Therefore, using small and focused libraries is often a more practical strategy for *in vivo* CRISPR screens (18).

Using an epigenetic-focused *in vivo* CRISPR screen in the KP lung ADC model, we studied the functions of epigenetic genes in modulating anti-tumor immunity, and identified anti-silencing function protein 1 homolog A (*Asf1a*) as a potential therapeutic target. ASF1 is a histone H3–H4 chaperone conserved from yeast to human cells. ASF1A and ASF1B are mammalian isoforms involved in DNA replication-coupled and DNA replication-independent nucleosome assembly pathways (22). ASF1 also plays a role in regulating gene transcription. For example, ASF1A resolves bivalent chromatin domains for the induction of lineage-specific genes during embryonic stem cell differentiation (23). Functional and mechanistic studies showed that *Asf1a* deficiency sensitizes lung ADC tumors to anti-PD-1 therapy by promoting M1-like macrophage polarization and enhancing T cell activation. Our findings provide a rationale for combining ASF1a inhibition and anti-PD-1 immunotherapy in lung ADC patients.

## RESULTS

### *In vivo* CRISPR screen identifies epigenetic regulators of tumor immunity

To systemically assess cell-intrinsic epigenetic regulators of tumor immunity, we developed an *in vivo* CRISPR screen using the KP mutant lung cancer mouse model (Fig. 1A). First, we generated an epigenetic-focused sgRNA library, which included sgRNAs targeting 524 epigenetic regulators and 173 control genes (essential genes, immune modulators), and non-targeting guides (Supplementary Table 1). We confirmed an even distribution of guides (Supplementary Fig. 1A). Next, we generated clonal KP mouse lung cancer cell lines with or without stable expression of Cas9 (Supplementary Fig. 1B), and confirmed Cas9 activity in KP-Cas9 clones (Supplementary Fig. 2A–C). We assessed the tumor formation capacity of library transduced KP-Cas9 clones (Supplementary Fig. 2D, E), and evaluated the sgRNA representation in tumors derived from KP clones (no Cas9) using the sgRNAs as barcodes (Supplementary Fig. 2F). KP-Cas9-clone 7 was selected for *in vivo* CRISPR screens because the clone showed superior Cas9 activity (Supplementary Fig. 2A) and maintained the optimal sgRNA representation *in vivo* (Supplementary Fig. 2F). Next, we injected early-passage KP-Cas9-clone 7 library cells into *Rag1*−/− and WT mice. On day 7, mice were treated with anti-PD-1 or isotype control. To identify changes in sgRNA abundances across

treatment groups, tumors were harvested on day 24 (12 tumors from 6 mice in each group), genomic DNA was isolated, and amplified sgRNA samples were prepared for next-generation sequencing (NGS). There were four treatment groups: immunodeficient *Rag1*−/− mice treated with control IgG (ID-IgG) or anti-PD-1 (ID-PD1), and immunocompetent WT mice treated with control IgG (IC-IgG) or anti-PD-1 (IC-PD1). Comparing sgRNAs recovered from tumors in B6 *Rag1*−/− and B6 WT mice treated with control IgG (ID-IgG VS IC-IgG), we identified epigenetic targets that, upon loss, modulated the anti-tumor immune response in the immunocompetent WT mice (Supplementary Fig. 3A, B; Supplementary Table 2). sgRNAs targeting Phosphatase and tensin homolog (*Pten*) were significantly enriched, and sgRNAs targeting Bromodomain-containing protein 4 (*Brd4*) were significantly depleted in anti-PD-1 treated WT hosts (Supplementary Fig. 3A). This is consistent with their dichotomous roles in regulating tumor immunity (24,25). Comparing sgRNAs recovered from tumors in B6 WT mice treated with control IgG and anti-PD-1 (IC-IgG VS IC-PD1), we identified targets that, when lost, either enhanced or inhibited sensitivity to anti-PD-1 treatment (Fig. 1B, C; Supplementary Table 2). As expected, sgRNAs targeting genes required for high expression of major histocompatibility complex class I (MHCI) (e.g., *Tap1*, *Tap2*, *B2m*, *Stat1*, *Jak1* or *Jak2*) promoted resistance to immunotherapy and were enriched in tumors treated with anti-PD-1 (Fig. 1B). By contrast, sgRNAs targeting *β-catenin* and *Mapk3* were significantly depleted (Fig. 1B), consistent with findings that *β-catenin* or *Mapk3* inhibition promotes sensitivity to ICB (26,27). Of note, sgRNAs targeting the histone chaperone gene anti-silencing function protein 1 homolog A (*Asf1a*) were also significantly depleted in tumors treated with anti-PD-1 (Fig. 1B–E). Importantly, *Asf1a* sgRNAs were only depleted by anti-PD-1 treatment in WT but not *Rag1*−/− mice and were not depleted by control IgG, suggesting specificity of responsiveness to PD-1 based immunotherapy and an enhanced T cell response (Fig. 1D). Based on these results, we hypothesized that *Asf1a* promotes suppression of tumor immunity.

### *Asf1a* deficiency enhances sensitivity to anti-PD-1 treatment

ASF1A is overexpressed in a variety of primary human tumors including lung ADC, and higher ASF1A expression is associated with a significantly poorer outcome in hepatocellular carcinoma patients (28). To evaluate the function of *Asf1a* in lung ADC, we established KP-Cas9 clones with *Asf1a* knockout (KO) (Supplementary Fig. 4A). *Asf1a* KO showed no obvious effect on the expression of its paralog gene *Asf1b* (Supplementary Fig. 4B). ASF1A inhibition can trigger DNA damage (28); however, we found that γH2AX levels showed no significant difference in KP cells with or without *Asf1a* KO (Supplementary Fig. 4C). To determine whether *Asf1a* KO alters the growth of KP lung tumors, we performed *in vitro* colony formation assay and an orthotopic xenograft experiment. *In vitro* colony formation assays showed no significant effect of *Asf1a* KO on tumor cell proliferation (Supplementary Fig. 4D, E). Orthotopic xenograft experiments also demonstrated that *Asf1a* KO had no effect on tumor growth in *Rag1*−/− mice (Supplementary Fig. 4F, G). Consistently, Using TCGA human lung cancer database, we found *ASF1A* expression shows no significant correlation with patient survival in either lung adenocarcinoma (LUAD) or lung squamous cancer (LUSC) (Supplementary Fig. 4H, I). However, using allograft experiments in WT mice we confirmed that *Asf1a* deficiency sensitizes tumors to anti-PD-1 treatment in

orthotopic lung cancer models (Fig. 2A–D). Using an inducible shRNA system, we further confirmed *Asf1a* knockdown (KD) exerted only a marginal effect on tumor cell proliferation (Supplementary Fig. 5A–C); however, *Asf1a* KD in combination with anti-PD-1 treatment significantly inhibited tumor growth in WT mice (Supplementary Fig. 5D–F). We also performed the treatment study in another KP model (KP-2) (Supplementary Fig. 6A–C). This model is very sensitive to anti-PD-1 treatment for as-yet-unclear reasons; however, *Asf1a* KO also showed significant synergistic effect with anti-PD-1 to inhibit KP-2 allograft tumors (Supplementary Fig. 6C). Collectively, these data confirmed our *in vivo* CRISPR screen results that *Asf1a* deficiency potentiated the effect of anti-PD-1 immunotherapy.

Additionally, we performed the treatment study in colon cancer model (MC38 allograft model), and found *Asf1a* KO significantly synergized with anti-PD-1 to inhibit MC38 allograft tumors (Supplementary Fig. 6D–G), suggesting that ASF1A loss might be a more wide-spread biomarker for susceptibility to anti-PD-1.

## Tumor cell-intrinsic *Asf1a* deficiency promotes M1-like macrophage polarization and T cell activation

To determine the mechanism by which loss of Asf1a enhances sensitivity to anti-PD-1, we evaluated the immune profile of orthotopic lung tumors following treatment (Supplementary Fig. 7). Targeting ASF1A or PD-1, alone or in combination, did not induce changes in the prevalence of $CD45^+$, $CD3^+$, $CD4^+$ and $CD8^+$ populations in the lung ADC tumor microenvironment (Supplementary Fig. 8A–D). Similarly, there was minimal correlation between *ASF1A* and *CD3D*, *CD4*, or *CD8A* expression in lung ADC samples in TCGA (Supplementary Fig. 8E–G). In addition, *Asf1a* KO or anti-PD-1 treatment alone showed a weak effect on the activation of effector T cells (Fig. 3A–D; Supplementary Fig. 8H–Q); however, *Asf1a* KO plus anti-PD-1 treatment markedly enhanced adaptive immunity (Fig. 3A–D; Supplementary Fig. 8H–Q). Moreover, Re-challenge experiment in MC38 allograft model showed re-challenged tumor cells grew more slowly in the *Asf1a* KO tumor bearing mice pretreated with anti-PD-1 comparing with Ctrl tumor bearing mice pretreated with anti-PD-1 (Supplementary Fig. 9A, B), which supports the existence of memory T cells in response to *Asf1a* loss. In addition, an *ex vivo* experiment showed that isolated pan T cells from the lungs of KP-*Asf1a KO* plus anti-PD-1 treatment group showed a stronger cytotoxicity to tumor cells when compared to those from spleens or lungs of Ctrl mice (Supplementary Fig. 9C), suggesting that T cells from combination group can specifically recognize tumor-associated antigens and result in cancer cell killing.

Furthermore, inflammatory monocytes and macrophage populations were significantly enriched in *Asf1a* KO tumors (Fig. 3E, F), whereas tumor-associated neutrophils (TAN), myeloid-derived suppressing cells (MDSC), eosinophils, $CD103^+$ DC and alveolar macrophage populations were not obviously affected (Supplementary Fig. 10A–G). Analysis of macrophage phenotypes demonstrated that the M1-like macrophages were significantly enriched in *Asf1a* KO tumors (Fig. 3G, H; Supplementary Fig. 10H, I). Furthermore, *Asf1a* KO in MC38 cells also significantly promoted GM-CSF transcription and increased the expression of M1 macrophage markers (IA/IE, CD80, CD86) in macrophages (Supplementary Fig. 6H–J). Collectively, these data suggested that *Asf1a* deficiency

sensitizes tumors to anti-PD-1 treatment by promoting M1-like macrophage polarization and T cell activation. This observation is consistent with our previous observations that M1-like macrophages promote T cell activation in cancer and enhance sensitivity to PD-1-based immunotherapy (29,30).

## Tumor cell-intrinsic *Asf1a* deficiency upregulates GM-CSF expression

To explore the mechanism by which *Asf1a* deficiency promotes M1-like macrophage polarization in lung ADC, we performed RNA sequencing (RNA-seq) on *Asf1a* KO and control KP cells. Gene set enrichment analysis (GSEA) revealed that the genes related to the TNFA signaling via NFKB and inflammatory response pathways were significantly enriched in KP cells with *Asf1a* KO (Fig. 4A–C; Supplementary Table 3). In parallel, we compared *ASF1A*-low lung ADC samples with *ASF1A*-high lung ADC samples in TCGA, and found TNFA signaling via NFKB and inflammatory response pathways were also significantly enriched in the *ASF1A*-low lung ADC samples (Figure 4D, E; Supplementary Table 3). Of note, GM-CSF (encoded by gene *Csf2*), an inflammatory cytokine in the TNFA pathway that promotes inflammatory monocytes infiltration and M1-like macrophage polarization (31,32), was significantly up-regulated in *Asf1a* KO KP cells (Fig. 4F–H). Similarly, we observed higher levels of GM-CSF in cell culture supernatant from *Asf1a* KO or KD KP cells (Fig. 4I; Supplementary Fig. 11A). Furthermore, analysis of mouse-derived organotypic tumor spheroids (MDOTS) revealed higher GM-CSF levels in *Asf1a* KO MDOTS (Supplementary Fig. 11B). Additionally, *Asf1a* KO in KP-2 cell line and MC38 cell line also promotes GM-CSF expression (Supplementary Fig. 6K, L).

ASF1A cooperates with chromatin assembly factor 1 (CAF-1) to promote replication-dependent chromatin assembly and with HIRA to promote replication-independent chromatin assembly (22), and nucleosome dynamics regulate gene transcription (33). Caf-1 subunits (*Chaf1a*, *Chaf1b*) and Hira were included in our sgRNA library, but the knockout of *Chaf1a*, *Chaf1b* or *Hira* did not sensitize to anti-PD-1 therapy in the screen (Supplementary Table 2). ATAC-seq data showed DNA accessibility of the *Csf2* gene did not differ among KP cells with or without *Asf1a* knockout (Supplementary Fig. 12A). However, chromatin immunoprecipitation sequencing (ChIP-seq) data in HeLa cells (34) showed that ASF1A occupies the promoter of *CSF2,* the gene encoding GM-CSF (Fig. 4J). Accordingly, *ASF1A* knockdown in human lung cancer cell line NCI-H2009 increased GM-CSF expression (Supplementary Fig. 12B, C), and ChIP-seq data in this cell line also showed the occupancy of ASF1A on the promoter of *CSF2* (Fig. 4K). These data support that ASF1A may directly inhibit the transcription of GM-CSF, independent of nucleosome assembly.

## *Asf1a* deficiency promotes innate and adaptive immunity via GM-CSF

To further evaluate how *Asf1a* deficiency in tumor cells promotes M1-like macrophage polarization, we co-cultured tumor cells with bone marrow macrophage precursors. *Asf1a* KO lung ADC cells significantly increased M1-like macrophage differentiation (Fig. 5A, B). To determine whether this effect is mediated by GM-CSF, we used a GM-CSF neutralizing antibody in the co-culture system, and observed a significantly reduced M1-like macrophage population under these conditions (Fig. 5C, D). These data suggest that tumor-intrinsic *Asf1a* loss promotes M1-like macrophage polarization through upregulation of GM-CSF. To

determine whether immunogenic macrophage differentiation, in turn, accounts for the enhanced T cell activation associated with *Asf1a* loss, we sorted macrophages from the tumor cell-bone marrow macrophage co-culture system and performed secondary co-culture with T cells. We observed that the macrophages entrained by *Asf1a* KO tumor cells promoted enhanced activation of T cells (Fig. 5E, F; Supplementary Fig. 13A–F). Collectively, these data indicate that tumor cell intrinsic *Asf1a* deficiency enhances M1-like macrophage polarization and promotes T cell activation via up-regulating GM-CSF.

To further evaluate the importance of GM-CSF mediated M1 macrophage polarization in anti-tumor immunity, we applied F4/80 and GM-CSF neutralizing antibodies during the *in vivo* treatment study. F4/80 antibody blocked the *Asf1a* KO plus anti-PD-1 treatment efficacy in 2 mice (2/6), and GM-CSF antibody blocked the *Asf1a* KO plus anti-PD-1treatment efficacy in 3 mice (3/6, 2 mice with high tumor burden died before week 3 MRI imaging) (Supplementary Fig. 14A). We found F4/80 or GM-CSF blockade inhibited T cell activation (Fig. 5G–L). Moreover, GM-CSF blockade also decreased the expression of M1 macrophage markers CD80, CD86 and IA/IE (Supplementary Fig. 14B–D). These data further support that GM-CSF up-regulation mediated M1 macrophage polarization plays pivotal roles in the anti-tumor immunotherapy.

## Single-cell analysis of intratumoral inflammatory cells confirms that combined targeting of *Asf1a* and PD-1 potentiates macrophage and T cell activation

The recent development of single-cell genomics has provided a powerful tool to dissect transcriptomic heterogeneity in tumor infiltrating immune cells (35,36). Therefore, to provide a comprehensive and unbiased assessment of immunotherapeutic responses affected by *Asf1a* deficiency or/and anti-PD-1 treatment, we performed single-cell RNA-seq (scRNA-seq) on lung ADC specimens. We harvested and pooled tumors from two mice in each group, and single suspension cells were collected and directly analyzed on the 10X Genomics platform. We identified distinct cancer cell, T cell, NK cell, B cell, macrophage/monocyte, dendritic cell (DC) and neutrophil clusters (Fig. 6A; Supplementary Fig. 15A, B). Consistent with our previous observations, there was an increase in the monocyte/macrophage cluster in tumors with *Asf1a* deficiency and/or anti-PD-1 treatment (Fig. 6B).

To further evaluate how *Asf1a* deficiency and anti-PD-1 immunotherapy affect the macrophage/monocytes transcriptome, we performed unbiased secondary clustering for these cells and identified 7 distinct subpopulations (Fig. 6C–E; Supplementary Fig. 16A, B). Cells in cluster MM_3 exhibited high *Itga4*, *Ly6c2*, *Ccr2* and *Cd62l* (*Sell)* expression, but low *Cx3cr1* expression (Supplementary Fig. 16A), resembling classical inflammatory monocytes (37–39). Cells in cluster MM_4 exhibited low *Ly6c2*, *Cd62l* (*Sell)* and *Ccr2* expression, but high *Itga4* and *Cx3cr1* expression (Supplementary Fig. 16A), consistent with a non-classical circulating monocyte phenotype (37–39). Cells in cluster MM_2 were characterized by the high *MHC-II (H2.Aa, H2.Ab1, H2.DMb1, H2.Eb1), Aif1, Tmem176a, Tmem176b, CD86, Ass1* and *Cxcl9* expression (Fig. 6E), characteristic of M1-like macrophages. *Asf1a* deficiency and/or anti-PD1 treatment markedly expanded the cluster 2 population. Cells in cluster MM_5 were defined by high-expression of *Arg1, Thbs1, Fn1 and Cd206 (Mrc1)* (Fig. 6E), which was associated with immune-suppressive M2-like

macrophages. Consistent with our previous observations, *Asf1a* deficiency and/or anti-PD1 treatment reduced the cluster MM_5 population (Fig. 6D).

To assess how *Asf1a* deficiency and anti-PD-1 immunotherapy affect the transcriptome of tumor-infiltrating T cells, we also performed unbiased secondary clustering of the bulk T cell population and identified 10 distinct subpopulations (Fig. 6F–H; Supplementary Fig. 17A, B). Cells in clusters T_2 and T_5 were characterized by the high expression of CD4 or CD8, as well as the high expression of *Cd62l* (Sell), but low expression of *Cd44* (Fig. 6H), consistent with naive T cell phenotype. *Asf1a* deficiency and/or anti-PD-1 immunotherapy decreased T_2 and T_5 populations (Fig. 6G). Cells in cluster T_1 were characterized by the high expression cytotoxic markers including *Cd8*, *Gzma*, *Gzmb*, *Gzmk* and *Prf1*, memory T cell markers including *Eomes* and *Fasl*, and T cell activation markers *Icos*, *Ifng*, *Ctla4*, *Lag3* and *Pdcd1* (Fig. 6H; Supplementary Fig. 17A), indicating a heterogeneous population containing memory and effector $CD8^+$ T cells. Anti-PD-1 immunotherapy increased T_1 population (Fig. 6G). Cluster T_4 shared similar signature with cluster T_1, but was characterized by highe *Ki67* (*Mki67*) expression (Fig. 6H), indicative of highly proliferative $CD8^+$ memory and effector T cells. *Asf1a* deficiency plus anti-PD-1 immunotherapy increased the T_4 population, which implies the memory and effector T cells started to expand from early time point (7 days). Cells in cluster T_9 have high expression of *Cd4* and T cell activation markers including *Icos*, *Ctla4*, *Tnfrsf4*, *Tnfrsf18*, *Tbet (Tbx21)*, *Pdcd1*, *Tnfrsf18* and *Tnfrsf4* (Fig. 6H; Supplementary Fig. 17A), indicative of Th1 cells. *Asf1a* deficiency plus anti-PD-1 immunotherapy increased the T_9 population (Fig. 6G), which is consistent with our previous observations (Supplementary Fig. 8L), supporting the enhanced M1 macrophage polarization. Cells in cluster T_3 and T_10 exhibited high expression of *Cd4*, *Foxp3* and *Il2ra* (Supplementary Fig. 17A), characteristic of regulatory T cells (Tregs). *Asf1a* deficiency plus anti-PD-1 immunotherapy increased T_3 and T_10 populations (Fig. 6G), possibly suggesting an acute positive feedback to a potentiated or activated tumor immune environment by short-term treatment.

In summary, these results support the notion that *Asf1a* deficiency and anti-PD-1 combination therapy restrains tumor progression through promoting inflammatory M1-like macrophage polarization and T cell activation.

## DISCUSSION

Compared to *in vitro* CRISPR screens, *in vivo* models are the more physiologically relevant systems to screen for new immunotherapy targets. Particularly, using small focused libraries is a practical strategy for *in vivo* CRISPR screens. Manguso *et al* first employed an *in vivo* CRISPR screen using an sgRNA sub-library containing ~2,000 selected genes to identify novel immunotherapy targets in melanoma (18). Our current study is the first *in vivo* CRISPR screen to identify novel immunotherapy targets in lung cancer utilizing an epigenetic sgRNA library containing 524 epigenetic genes. Internal quality controls indicated that our *in vivo* CRISPR screen functioned successfully, and our study provided further proof of principle for the utilization of *in vivo* CRISPR screens for detecting potential targets for cancer immunotherapy.

The development of immune checkpoint targeted antibodies has brought hope to some advanced-stage *KRAS*-mutant lung ADC patients, but the majority of patients remain unresponsive to immunotherapy. The modest response rates highlight an urgent need for new therapeutic approaches to augment the anti-tumor immune response. Our *in vivo* epigenetic CRISPR screen identified *Asf1a* as an immunotherapeutic target whose inhibition synergizes with anti-PD-1 treatment by promoting M1-like macrophage differentiation and enhancing T cell activation. Our results thus provide rationale for combination therapy consisting of ASF1A inhibition and anti-PD-1 immunotherapy for lung ADC patients. Unfortunately, we could not access any human lung cancer patient data with immune checkpoint-blockade treatment to analyze whether ASF1A loss is a biomarker for immune checkpoint blockade. It would be very interesting if we could use this finding to strategize treatment of cancer patient based on their ASF1A expression levels, and to see whether ASF1A-low patients treated anti-PD-1 antibody will have better outcome and survival.

*Asf1a* plays a role in regulating gene transcription (23), but its function in cancer has been only scarcely studied. Individual reports showed that ASF1A inhibition elicits DNA damage in cancer cells (28). While emerging evidence indicates that accumulated DNA damage may lead to increased inflammation through the cGAS-cGAMP-STING pathway (40), we found no significant difference in γH2AX levels in KP cells with or without *Asf1a* knockout, indicating that the enhanced inflammation in *Asf1a* knockout tumors might not be due to the DNA damage response. Transcriptional profiling revealed that *Asf1a* depletion led to the up-regulation of a variety of factors, including GM-CSF, which was confirmed in cell culture supernatants. Furthermore, the ChIP-seq data confirmed the occupancy of ASF1A on the promoter of *CSF2*. GM-CSF (encoded by *CSF2*) promotes M1-like macrophage differentiation (31,32). Thus, our data reveal a mechanism for the increased abundance of M1-like macrophages in *Asf1a*-deficient tumors.

The function of GM-CSF in anti-tumor immunity is controversial. GM-CSF plays an important role in dendritic cell (DC) development (41), and DCs are critical in T cell priming. Moreover, GM-CSF was reported to promote the M1 macrophage polarization (42), and M1 macrophages promote anti-tumor immunity. By contrast, tumor-derived GM-CSF is necessary and sufficient to drive the development of $CD11b^{+}Gr1^{+}$ MDSCs that suppressed antigen-specific T cells, and thus promotes tumor progression (43,44). However, in our model, although *Asf1a* KO-induced elevation of GM-CSF expression did not increase the MDSC population in the tumor microenvironment (Supplementary Fig. 10C), it's still unclear whether overall GM-CSF blockade will inhibit the suppressive function of MDSCs. It is hard to segregate tumor-derived GM-CSF versus overall GM-CSF systemically in the current study. Moreover, GM-CSF works in concert with other chemokines/cytokines to promote the suppressive function of MDSCs (45), and the alterations of other chemokines/cytokines may be also involved in the regulation of MDSC population in our model.

Elevated expression of MHC class II in tumor-associated macrophages promotes antigen presentation and T cell priming (14). In line with this, our data revealed an up-regulation of MHCII in tumor-associated macrophages (increased M1-like macrophage) in *Asf1a*-deficient tumors, which could potentially enhance T cell activation and augment sensitivity to anti-PD-1 immunotherapy.

Interestingly, *Asf1a* deficiency alone did not robustly reduce tumor progression in our KP orthotopic allograft model, suggesting that increased M1-like macrophage differentiation may not be sufficient to achieve a sustained anti-tumor immune response. However, tumor cell-intrinsic *Asf1a* deficiency coupled with anti-PD-1 treatment substantially increased the anti-tumor immune response. In *Asf1a*-deficient tumors treated with anti-PD-1, we observed a decrease in CD62L expression coupled with an increase in CD69, 4–1BB, OX40 and ICOS expression on intratumoral T cells, suggesting the enhanced T cell activation in this context. These data suggest that combined targeting of *Asf1a* and PD-1 may enable the efficacy for targeting addition checkpoint or costimulatory receptors.

Our study focused on the macrophage population, but we could not exclude the possibility that the other immune populations, such as dendritic cells, neutrophils and natural killer cells, may also play important roles in the anti-tumor immune response in *Asf1a*-deficient tumors treated with anti-PD-1. ScRNA-seq analyses of intratumoral immune populations revealed an increase in DCs and NK cells and decrease in neutrophils. GM-CSF promotes inflammatory monocyte differentiation into dendritic cells (41), which play critical roles in antigen presentation and T cell priming (46). NK cells also play important roles in the anti-tumor immune response (47). By contrast, tumor-associated neutrophils inhibit the anti-tumor immune response (48), and decreased neutrophil levels support enhanced anti-tumor immune responses. Thus, the mechanism of the enhanced anti-tumor immune response in *Asf1a*-deficient tumors treated with anti-PD-1 may involve multiple innate immune populations. Future work is needed to address whether Asf1a can directly affect the activity of immune cells.

The development of a specific ASF1A inhibitor will potentially facilitate the translational significance of current work. Seol *et al* developed multiple ASF1A inhibitors and tested them *in vitro* (49). However, a high concentration (30uM-50uM) of these inhibitors was required to interrupt the interaction between ASF1A and histone H3. In HeLa cells, only a high concentration (40 uM) treatment with the putative inhibitors could inhibit H3K56 acetylation. These compounds were not fully optimized for targeting ASF1A, and there are no data from *in vivo* studies to support their targeting efficacy. Further effort is needed to optimize the drug with lower IC50 and better pharmacodynamic efficacy for *in vivo* testing and clinical applications.

ASF1A inhibition may cause cell cycle arrest in some cell types (28). As in the case of CDK4/6 inhibition, despite the fact that CDK4/6 inhibitors can cause cell cycle arrest even in some normal cell types and immune cells, they were still approved by the FDA for the treatment of certain patients with breast cancer (50). Besides causing cell cycle arrest, CDK4/6 inhibitors could also affect other aspects of cancer cell behavior such as enhancing anti-tumor immunity if dosing schedule is optimized as intermittent to bypass the cell cycle arrest (51,52), suggesting that CDK4/6 is still an attractive therapeutic target. Similarly, beyond the possible cell cycle arrest in some cell types (28), here we showed that ASF1A is a potential target and its inhibition can synergize with anti-PD-1 treatment to restrain cancer development with enhance anti-tumor immunity through both macrophage and T cells. There is a need to develop more efficient and selective ASF1A inhibitors for further pre-clinical and clinical evaluation of the feasibility of targeting ASF1A in lung cancer and other

cancers. Upon drug optimization, further investigations of the treatment strategy are needed to minimize the cell cycle arrest side effect of ASF1A inhibition.

In summary, we performed an in vivo epigenome-focused CRISPR screen and identified ASF1A as a promising candidate in sensitizing immunotherapy. Functional and mechanistic studies showed that tumor cell intrinsic *Asf1a* deficiency promotes inflammation and M1-like macrophage polarization and further promotes T cell activation in combination with anti-PD-1 treatment (Fig. 7). ASF1A loss combined with anti-PD-1 treatment exerted significant inhibition on tumor growth. Thus, combining ASF1A inhibition with immune checkpoint blockade such as anti-PD-1 treatment might serve as a potential novel immunotherapy strategy for lung cancer patients.

## METHODS

### Cell culture, plasmid construction, and lentivirus infection

HEK-293T cells and colon cancer cell line MC38 were cultured in Dulbecco's Modified Eagle Medium (DMEM, Gibco) with 10% fetal bovine serum (FBS). Mouse lung ADC line KP and KP-2 (C57BL/6 background), and human lung ADC cell line NCI-H2009 were cultured in Roswell Park Memorial Institute (RPMI) 1640 (Gibco) with 10% FBS. All cell lines used in this study were tested as mycoplasma negative using Universal Mycoplasma Detection Kit (ATCC® 30–1012K™). Plasmids pLenti-Cas9-Puro, pXPR-GFP-Blast, pLKO.1-Tet-on, PSPAX2 and PMD2.G were purchased from Addgene.

The sgRNAs specific for mouse *Asf1a* were cloned into pXPR-GFP-Blast vector using Gibson Assembly kit (E2611L, NEB). The target sequences are as follows;

sg*Asf1a*-1: 5'-CTGATTACTTGCACCTACCG-3'

sg*Asf1a*-2: 5'-TCTGGGATGAGTCCTGCATT-3'

sg*Asf1a*-3: 5'-GATCACCTTCGAGTGCATCG-3'

sg*Asf1a*-4: 5'-TAGGCTGATGCACCGAATGC-3'

The shRNAs specific for mouse *Asf1a* were cloned into pLKO.1-Tet-on vector with the AgeI/EcoRI sites. The target sequences are as follows;

sh*Asf1a*-2: 5'-CTAAGCTTCAAAGGAATATTT-3'

sh*Asf1a*-3: 5'-TGAGCAAATTGTGGATTATAA-3'

The shRNAs specific for human *ASF1A* (pLKO.1 vector) were purchased from Sigma. The target sequences are as follows;

sh*ASF1A*-1: 5'-GCCAGATGTTAAACTTTGAAT-3' (TRCN0000074268)

sh*ASF1A*-4: 5'-AGGCGTAACTGTTGTGCTAAT-3' (TRCN0000074271)

To generate lentivirus, HEK-293T cells were co-transfected with pLenti-Cas9, pXPR-GFP-sgRNA-Blast, or pLKO.1-Tet-on-shRNA plasmid, and packaging plasmids PSPAX2 and PMD2.G using Lipofectamine 3000 (Invitrogen). Viral particles released into the cell culture supernatant were filtered with 0.45-μm filters (Corning) to remove cellular debris. KP cells were transduced by culturing with viral supernatants in the presence of polybrene (Sigma) to increase infection efficiency. Stable cell lines were selected and maintained in cell culture media containing 2 μg/mL puromycin or 5 ug/mL blasticidin.

### Colony formation assay

Cells were trypsinized to produce a single-cell suspension. 1000 cells were counted and plated in each well of 6-well plate. Medium was changed every two days. After 9 days, cells were fixed with 70% ethanol for 10 minutes, and the cells were stained with 0.5% crystal violet (dissolved in 20% methanol) for 5 minutes and washed. Photos were taken and quantified using ImageJ.

### Construction of an epigenetic focused sgRNA library

We obtained sgRNA oligo pools from the Belfer Center for Applied Cancer Science at the Dana-Farber Cancer Institute (53). The library contains 7780 sgRNAs, including sgRNAs targeting 524 epigenetic regulators, 173 control genes (essential genes, immune modulators, etc), and 723 non-targeting sgRNAs. For each gene, there are 8–12 sgRNAs. Additional details of the library are included in Supplementary Table 1.The sgRNA library was inserted into the pXPR-GFP-Blast vector using the Gibson assembly kit (NEB), expanded by transformation into electrocompetent cells (Invitrogen) by electroporation. Library representation was maintained at least 1000x at each step of the preparation process.

### *In vivo* screen using a KP-Cas9 lung cancer cell line in B6 mice

We isolated single clones from a KP lung cancer cell line with pure C57BL/6 background. To determine how propagation as a tumor *in vivo* affects basal sgRNA library distribution, clones without Cas9 expression were transduced at a low multiplicity of injection (MOI) with the sgRNA library for use as barcodes. Following several days of expansion in medium with 5 ug/mL blasticidin, a pellet of at least 8 million cells was kept to evaluate the initial sgRNA distribution and the remainder was injected subcutaneously into B6-*Rag1*−/− and B6 WT mice. Tumors were allowed to grow to 500 $mm^3$, then excised for NGS analysis to evaluate the final library distribution. For the functional screen, KP-Cas9 cells were generated by viral transduction and Cas9 expression was confirmed by western blot. Cas9-mediated DNA editing was confirmed using sgRNAs targeting the essential gene *Rbx1*. KP-Cas9 clones with validated Cas9 activity were transduced at a MOI of 0.2 with lentivirus produced from the libraries with at least 1,000-fold coverage (cells per construct) in each infection replicate. Transduced KP cells were expanded *in vitro* for 2 weeks and then subcutaneously implanted into B6-*Rag1*−/− mice and C57BL/6 mice. These mice were then treated with anti-PD-1 or isotype control (3 times per week) on day 7 when the average tumor size reached 60 $mm^3$, tumors were harvested on day 24 when the tumor size was roughly 500 $mm^3$. To better keep the *in vivo* sgRNA representations, there are 12 tumors from 6 mice in each group. Genomic DNAs of tumors or cells were extracted using the DNA

Blood Midi kit (Qiagen). PCR was used to amplify the sgRNA cassette, and NGS sequencing was performed on an Illumina HiSeq to determine sgRNA abundance.

## Data analysis for CRISPR screen

Adaptor sequences were trimmed using cutadapt (v1.18), and untrimmed reads were removed. Then sequences after the 20-base gRNAs were cut using fastx-toolkit (v0.0.13) (http://hannonlab.cshl.edu/fastx_toolkit/index.html), gRNAs were mapped to the annotation file (0 mismatch), and read count tables were made. The count tables were normalized based on their library size factors using DESeq2 (54), and differential expression analysis was performed. Further, MAGeCK (0.5.8) (55) was used to normalize the count table based on median normalization and fold changes, and significance of changes in the conditions was calculated for genes and sgRNAs. Pathway analysis and Gene Set Enrichment Analysis (GSEA) were performed using ClusterProfiler R package (v3.6.0) (56). All downstream statistical analyses and generating plots were performed in R (v3.1.1) (http://www.r-project.org).

## Animal studies

All mouse work was reviewed and approved by the Institutional Animal Care and Use Committee (IACUC) at either NYU School of Medicine or Dana-Farber Cancer Institute. Specific-pathogen-free facilities were used for housing and care of all mice. Six-week old male B6-*Rag1*$^{-/-}$ and B6 WT mice were purchased from Jackson Laboratories. For screen, $8.0\times10^6$ library-transduced KP-Cas9 cells were resuspended in phosphate buffered saline (PBS) and subcutaneously inoculated into the flanks of B6 mice. Mouse anti-PD-1 ab (29F.1A12) (57) or isotype control was administered 3 times per week (Monday, Wednesday, and Friday) at 200 μg/mouse via intraperitoneal injection. Tumor size was measured every 3 days using calipers to collect maximal tumor length and width. Tumor volume was estimated with the following formula: $(L \times W^2)/2$.

For the single nodule orthotropic lung cancer model, 0.25 million cells in 20 uL PBS were injected into the left lung through the ultrasound guided trans-thoracic injection. Tail vein injection was also used here as an alternative orthotopic model, and 1 million cells were injected into each mouse. Magnetic resonance imaging (MRI) was used to monitor tumor formation and progression in orthotopic models. Randomization of mouse groups was performed when appropriate. Mice were treated with isotype control, anti-PD-1 antibody (29F.1A12) (57). For F4/80 or GM-CSF blocking study, mice were injected intraperitoneally with either anti-F4/80 antibody (200 ug, clone CI:A3–1, Bio X Cell) or anti-GM-CSF antibody (200 ug, clone MP1–22E9, Bio X Cell) 48 and 24 hours before the beginning of anti-PD-1 treatment of KP-Asf1a KO tumors, and 3 times per week thereafter. $CO_2$ inhalation was used to euthanize mice when we harvested the tissues.

## MRI quantification

Mice were anesthetized with isoflurane to perform lung MRI using BioSpec USR70/30 horizontal bore system (Bruker) to scan 24 consecutive sections. Tumor volume within the whole lung was quantified using 3-D slicer software to reconstruct MRI volumetric

measurements, as described previously (58). Acquisition of the MRI signal was adapted according to cardiac and respiratory cycles to minimize motion effects during imaging.

### RNA-seq and data analyses

RNA-seq on KP cells with or without *Asf1a* KO was performed in NYU Langone Medical Center Genome Technology Core. STAR 2.4.2a (59) was used to align the RNA-seq samples to the reference mouse genome (mm9) and to count the number of reads mapping to each gene in the ensembl GRCm38.80 gene model. Differential expression between the different groups was performed through the use of DESeq2 (60). Differential-expression analysis was done using R (v.3.5.1) (http://www.R-project.org/) and the DESeq2 package (v.1.10.0).

Gene set enrichment analysis was done using GSEA (v.3.0) and gene sets from MSigDB (v. 5.0). We used the 'preranked' algorithm to analyze gene lists ranked by the negative decadic logarithm of P values multiplied by the value of log2FC obtained from the differential-expression analysis with DESeq2.

### TCGA RNA-seq data analysis

Level 3 RNA-seq data for TCGA lung adenocarcinomas were obtained through the TCGA portal. Data were sorted based on the expression level of *ASF1A*, and the samples were separated into quarters. The top 25% expression group (high expression) was compared with the low 25% expression group (low expression) by GSEA analysis as outlined in the RNA-seq data analysis section. The gene list for GSEA input was ranked by the value of log2FC, where FC is defined by the ratio of low expression: high expression.

### ChIP-seq and ATAC-seq

Chromatin immunoprecipitation (ChIP) was performed in human lung cancer cell line NCI-H2009 using Pierce Magnetic ChIP Kit (26157, Thermo scientific) following the manufacturer's instructions. Antibody against Asf1a (2990s, Cell Signaling Technology) was used. ChIP DNA was purified and sent to NYULH Genome Technology Center for library construction and sequencing.

For ATAC-seq, freshly harvested cells were directly sent to NYULH Genome Technology Center for library construction and sequencing.

### ChIP-Seq and ATAC-Seq data analysis

All of the reads from the sequencing experiment were mapped to the reference genome using the Bowtie2 (v2.2.4) (61) and duplicate reads were removed using Picard tools (v. 1.126) (http://broadinstitute.github.io/picard/). Low-quality mapped reads (MQ<20) were removed from analysis. The read per million (RPM) normalized BigWig files were generated using BEDTools (v.2.17.0) (62) and the bedGraphToBigWig tool (v.4). Peak calling was performed using MACS (v1.4.2) (63) and peak count tables were created using BEDTools. Differential peak analysis was performed using DESeq2 (54). ChIPseeker (v1.8.0) (64) R package was used for peak annotations and motif discovery was performed using HOMER (v4.10) (65). ngs.plot (v2.47) (65) and ChIPseeker were used for TSS site visualizations and quality controls. KEGG pathway analysis and Gene Ontology (GO)

analysis was performed using the clusterProfiler R package (v3.0.0) (56). To compare the level of similarity among the samples and their replicates, we used two methods: principal-component analysis and Euclidean distance-based sample clustering. Downstream statistical analyses and generating plots were performed in R environment (v3.1.1) (https://www.r-project.org/).

### Tumor-infiltrating immune cell isolation and FACS analysis

Mice were euthanized, and lungs were perfused with sterile PBS through heart perfusion from the left ventricle after collection of bronchoalveolar lavage (BAL) fluid. Whole lung was minced and digested in collagenase D (11088866001, Roche) and DNase I (10104159001, Roche) in Hank's Balanced Salt Solution at 37°C for 30 minutes. After incubation, digested tissue was filtered through a 70-μm cell strainer (Thermo Fisher Scientific) to obtain single-cell suspensions. Separated cells were treated with 1× RBC lysis buffer (BioLegend) to lyse red blood cells. Live cells were determined with a LIVE/DEAD Fixable Aqua Dead Cell Stain kit (Molecular Probes). Cell pellets were resuspended in PBS with 2% FBS for FACS analysis. Cells were stained with the indicated cell surface markers and fixed/permeabilized using a Fixation/Permeabilization kit (eBioscience). Cells were imaged on a BD Biosciences LSRFortessa and analyzed with FlowJo software. The gating strategy was described previously (66).

### Flow antibodies

Lung-infiltrating immune cells were stained with fluorochrome-coupled antibodies against mouse CD45 (clone 30-F11, BioLegend), CD3 (clone 17A2, BioLegend), CD4 (clone GK1.5, BioLegend), CD8 (clone 53–6.7, BioLegend), CD44 (clone IM7, BioLegend), CD62L (clone MEL-14, Biolegend), CD69 (clone H1.2F3, BioLegend), 4–1BB (CD137, clone 17B5, Biolegend), GITR (CD357, clone DTA-1, BioLegend), GZMB (clone GB11, BD Horizon), OX40 (CD134, clone OX-86, BioLegend), ICOS (clone 7E.17G9, BD OptiBuild), CD11b (clone M1/70, BioLegend), CD11c (clone N418, BioLegend), Ly-6G (clone 1A8, BioLegend), SiglecF (Clone E50–2440, BD Pharmingen), Ly-6C (clone HK1.4, BioLegend), Gr1 (Ly-6G/Ly-6C, clone RB6–8C5, BioLegend), CD103 (clone 2E7, BioLegend), F4/80 (clone BM8, BioLegend), CD80 (clone 16–10A1, BioLegend), CD86 (clone GL-1, BioLegend), IA/IE (clone M5/114.15.2, Biolegend) and CD206 (clone C068C2, BioLegend).

### Single-cell RNA sequencing

Single-cell suspensions were achieved as described above and sorted using DAPI staining. Cells were then resuspended into single cells at a concentration of $1 \times 10^6$ per mL in 1X PBS with 0.4% BSA for 10x genomics processing. Cell suspensions were loaded onto a 10x Genomics Chromium instrument to generate single-cell gel beads in emulsion (GEMs). Approximately 5,000 to 10,000 cells were loaded per channel. scRNA-seq libraries were prepared using the following Single Cell 3′ Reagent Kits: Chromium™ Single Cell 3′ Library & Gel Bead Kit v2 (PN-120237), Single Cell 3′ Chip Kit v2 (PN-120236) and i7 Multiplex Kit (PN-120262) (10x Genomics, Pleasanton, CA, USA) as previously described (67), and following the Single Cell 3′ Reagent Kits v2 User Guide (Manual Part # CG00052 Rev A). Libraries were run on an Illumina HiSeq 4000 system (SY-401–4001, Illumina) as 2

× 150 paired-end reads, one full lane per sample, for approximately >90% sequencing saturation.

## Single cell RNA-seq data analysis

After confirming the integrity of the cDNA, quality of the libraries, number of cells sequenced and mean number of reads per cell, as a quality control, we used the cellranger package to map the reads and generate gene-cell matrices. A quality control was then performed on the cells to calculate the number of genes, UMIs and the proportion of mitochondrial genes for each cell using iCellR R package (v0.99.0) (https://github.com/rezakj/iCellR) and the cells with low number of covered genes (gene-count < 500) and high mitochondrial counts (mt-genes > 0.1) were filtered out. Following this, the matrix was normalized based on ranked geometric library size factor (ranked glsf) using iCellR. Geometric library size factor normalization is a common normalization method used by popular tools such as DEseq2 (54), however, here we use only the top ranked genes (top 500 genes sorted by base mean) this is for reducing the effect of dropouts (nonzero events counted as zero) in normalization by taking into account only the highly expressed genes. A general gene statistics was then performed to calculate gene dispersion, base mean and cell coverage to use to build a gene model for performing Principal Component Analysis (PCA). Genes with high coverage (top 500) and high dispersion (dispersion > 1.5) were chosen and PCA analysis was performed, a second round of PCA was performed based on the top 20 and bottom 20 genes predicted in the first 10 dimensions of PCA to fine tune the results and clustering was performed (iCellR options; clust.method = “kmeans”, dist.method = “euclidean”, index.method = “silhouette”) on principal component with high standard deviation (top 10 PCs) and T-distributed Stochastic Neighbor Embedding (t-SNE) was performed. Uniform Manifold Approximation and Projection (UMAP) was also performed on the top 10 PCs. Marker genes for each cluster were determined based on fold change and adjusted p-value (t-test) and average gene expression for each cluster was calculated using iCellR. Marker genes were visualized on heatmaps, bar plots and box plots for each cluster and were used to determine the cell types using ImmGen database (https://www.immgen.org/).

## Western blots and antibodies

Cells were lysed in RIPA buffer (Pierce) containing protease/phosphatase inhibitor cocktail (Thermo Scientific). Protein concentration was measured using the BCA assay (Pierce). Equivalent amounts of each sample were loaded on 4%–12% Bis-Tris gels (Invitrogen), transferred to nitrocellulose membranes, and immunoblotted with antibodies directed against Cas9 (MA1–202, ThermoFisher), Asf1a (2990s, Cell Signaling Technology), Asf1b (PA5–67639, Invitrogen), γH2AX (9718s, CST) and β-actin (Ab8227, Abcam). IRDye 800-labeled goat anti-rabbit IgG and IRDye 680-labeled goat anti-mouse IgG secondary antibodies were purchased from LI-COR Biosciences, and membranes were detected with an Odyssey detection system (LI-COR Biosciences).

## Luminex analyses

Cell culture medium was harvested 30 hours after seeding cells. Murine-derived organotypic tumor spheroids (MDOTS) was performed as previously described (68), and culture medium

was harvested 3 days post-treatment. Cytokine/chemokine profiling of cell culture medium was performed using a Milliplex MAP Kit (Millipore) and measured on Multiplex Analyzer (Millipore). Concentrations (pg/mL) of each protein were derived from 5-parameter curve fitting models. Fold changes relative to the control were calculated and plotted as log2-fold change. Lower and upper limits of quantitation (LLOQ/ULOQ) were derived from standard curves for cytokines above or below detection.

### *In vitro* co-culture assay

Bone marrow derived macrophages (BMDMs) were prepared and cultured as previously described (30). In select experiment, tumor cells and bone marrow cells were mixed and plated in a well of a 6-well plate at a ratio of 2:3 (0.4 million: 0.6 million). Cells were grown in RPMI-1640 with 10% FBS and 1 ng/mL MCSF, and medium was changed every 2 days. After 7 days of co-culture, cells were harvested for immunostaining and FACS analyses.

For T cell activation experiment, $GFP^{-}/DAPI^{-}/CD11b^{+}/Gr1^{-}/F4/80^{+}$ macrophage cells from the above co-culture system were sorted, stimulated with Ova 257–264 peptide (10ug/ml, 1 hour), and then further co-cultured with OT-I T cells in a 1:5 ratio (0.025 million Macrophages: 0.125 million T cells) in a 96-well U bottom plate and T cell activation medium was used. After 5 days of co-culture, OT-I T cells were directly used for immunostaining and flow cytometry analysis.

B6 WT mice were intravenously injected with KP-Ctrl or KP-*Asf1a* KO cells, and tumor formation in the lung was indicated by MRI imaging. These mice were treated with PD-1 ab for 1 week (3 times per week). Pan T cells from the spleens or lungs of these pre-treated mice were isolated using Pan T cell Isolation Kit (Mouse, 130–095-130), and co-cultured with KP-Ctrl tumor cells in a 1:3 ratio (0.12 million T cells: 0.36 million tumor cells). After 2 days of co-culture, Cell Counting Kit-8 (ALX-850–039-KI02, Enzo) was used to measure tumor cell activity.

### Rechallenge experiment

1 million MC38-Ctrl or MC38-*Asf1a* cells were subcutaneously injected to the left flanks of mice. When the average tumor size reached 120 $mm^3$, mice were treated with anti-PD-1 for 2 weeks. Following treatment, 1 million MC38-Ctrl cells were subcutaneously injected to the right flanks of pre-treated mice bearing MC38-Ctrl tumors or MC38-*Asf1a* KO tumors. After 8 days, tumors on the right flanks were measured and harvested for further analysis.

### Quantitative RT-PCR

Total RNA was extracted from cells using an RNeasy Plus Mini Kit (Qiagen), and cDNA was generated with a High-Capacity cDNA Reverse Transcription Kit (Applied Biosystems). Quantitative PCR was performed using SYBR Green PCR Master Mix (Applied Biosystems), and transcript levels were normalized to the internal control, actin. Samples were run in triplicate. The primer sequences are as follows:

m*Asf1a*-F: 5’- ATGTGGGCTCTGCAGAAAGT-3’

m*Asf1a*-R: 5’- CTGTTACCCCCACTGCATCT-3’

h*ASF1A*-F: 5’- CCTTTCTACAACCCGTTCCA-3’

h*ASF1A*-R: 5’- ACTTTCTGCAGAGCCCACAT -3’

m*Csf2*-F: 5’- ATGCCTGTCACGTTGAATGA-3’

m*Csf2*-R: 5’- CCGTAGACCCTGCTCGAATA-3’

h*CSF2*-F: 5’- TTCTGCTTGTCATCCCCTTT-3’

h*CSF2*-R: 5’- CTTGGTCCCTCCAAGATGAC-3’

m*Actin*-F: 5’- CTGTCCCTGTATGCCTCTG-3’

m*Actin*-R: 5’- ATGTCACGCACGATTTCC-3’

h*ACTIN*-F: 5’-CACCATTGGCAATGAGCGGTTC-3’

h*ACTIN*-R: 5’-AGGTCTTTGCGGATGTCCACGT-3’

### Statistical analysis

All statistical analyses were carried out using GraphPad Prism 7. Data were analyzed by Student’s t-test (two tailed). Survival was measured according to the Kaplan-Meier method and analyzed by log rank (Mantel-Cox) test. $P < 0.05$ was considered significant. Error bars represent standard error of the mean (SEM).

### Data access

NGS data for CRISPR screen, RNA-seq data, single-cell RNA-seq data, ChIP-seq data and ATAC-seq data have been deposited in the National Center for Biotechnology Information’s Gene Expression Omnibus and are accessible through GEO Series accession number GSE127205 (https://www.ncbi.nlm.nih.gov/geo/query/acc.cgi?acc=GSE127205), GSE127232 (https://www.ncbi.nlm.nih.gov/geo/query/acc.cgi?acc=GSE127232), GSE133604 (https://www.ncbi.nlm.nih.gov/geo/query/acc.cgi?acc=GSE133604), and GSE138571 (https://www.ncbi.nlm.nih.gov/geo/query/acc.cgi?acc=GSE138571).

## Supplementary Material

Refer to Web version on PubMed Central for supplementary material.

## ACKNOWLEDGEMENTS

We thank the NYU Langone Medical Center and Dana-Farber Cancer Institute Animal Resources Facility staff for their support of the animal studies. We thank the Dana-Farber Cancer Institute Genome Technology Core for NGS sequencing of CRISPR screen. We thank the NYU Langone Medical Center Genome Technology Center for NGS-seq of CRISPR screen samples, RNA-seq, ATAC-seq, ChIP-seq and scRNA-seq. We thank the NYU Langone Medical Center Cytometry & Cell Sorting Laboratory for FACS analyses and cell sorting service. We thank the NYU Langone Medical Center Applied Bioinformatics Laboratories for bioinformatics analyses. We thank the NYU Langone Medical Center Preclinical imaging Laboratory for providing ultrasound and MRI equipments. This work was supported by NIH funding CA233084-01 (to K.K.W.), CA219670-A1 (to K.K.W), CA216188-01A1 (to K.K.W.), CA222218-A1 (to J.Q.) and P50CA101942 (to G.J.F).

## REFERENCES


1. Siegel RL, Miller KD, Jemal A. Cancer statistics, 2019. CA Cancer J Clin 2019;69(1):7–34 doi 10.3322/caac.21551. [PubMed: 30620402]
2. Cancer Genome Atlas Research N. Comprehensive molecular profiling of lung adenocarcinoma. Nature 2014;511(7511):543–50 doi 10.1038/nature13385. [PubMed: 25079552]
3. Paez JG, Janne PA, Lee JC, Tracy S, Greulich H, Gabriel S, et al. EGFR mutations in lung cancer: correlation with clinical response to gefitinib therapy. Science 2004;304(5676):1497–500 doi 10.1126/science.1099314. [PubMed: 15118125]
4. Lynch TJ, Bell DW, Sordella R, Gurubhagavatula S, Okimoto RA, Brannigan BW, et al. Activating mutations in the epidermal growth factor receptor underlying responsiveness of non-small-cell lung cancer to gefitinib. N Engl J Med 2004;350(21):2129–39 doi 10.1056/NEJMoa040938. [PubMed: 15118073]
5. Pao W, Miller VA. Epidermal growth factor receptor mutations, small-molecule kinase inhibitors, and non-small-cell lung cancer: current knowledge and future directions. J Clin Oncol 2005;23(11): 2556–68 doi 10.1200/JCO.2005.07.799. [PubMed: 15767641]
6. Janes MR, Zhang J, Li LS, Hansen R, Peters U, Guo X, et al. Targeting KRAS Mutant Cancers with a Covalent G12C-Specific Inhibitor. Cell 2018;172(3):578–89 e17 doi 10.1016/j.cell.2018.01.006. [PubMed: 29373830]
7. Lito P, Solomon M, Li LS, Hansen R, Rosen N. Allele-specific inhibitors inactivate mutant KRAS G12C by a trapping mechanism. Science 2016;351(6273):604–8 doi 10.1126/science.aad6204. [PubMed: 26841430]
8. Ostrem JM, Peters U, Sos ML, Wells JA, Shokat KM. K-Ras(G12C) inhibitors allosterically control GTP affinity and effector interactions. Nature 2013;503(7477):548–51 doi 10.1038/nature12796. [PubMed: 24256730]
9. Singh H, Longo DL, Chabner BA. Improving Prospects for Targeting RAS. J Clin Oncol 2015;33(31):3650–9 doi 10.1200/JCO.2015.62.1052. [PubMed: 26371146]
10. Sharma P, Allison JP. The future of immune checkpoint therapy. Science 2015;348(6230):56–61 doi 10.1126/science.aaa8172. [PubMed: 25838373]
11. Skoulidis F, Goldberg ME, Greenawalt DM, Hellmann MD, Awad MM, Gainor JF, et al. STK11/LKB1 Mutations and PD-1 Inhibitor Resistance in KRAS-Mutant Lung Adenocarcinoma. Cancer Discov 2018;8(7):822–35 doi 10.1158/2159-8290.CD-18-0099. [PubMed: 29773717]
12. Pardoll DM. The blockade of immune checkpoints in cancer immunotherapy. Nat Rev Cancer 2012;12(4):252–64 doi 10.1038/nrc3239. [PubMed: 22437870]
13. Esteller M Epigenetics in cancer. N Engl J Med 2008;358(11):1148–59 doi 10.1056/NEJMra072067. [PubMed: 18337604]
14. Adeegbe DO, Liu Y, Lizotte PH, Kamihara Y, Aref AR, Almonte C, et al. Synergistic Immunostimulatory Effects and Therapeutic Benefit of Combined Histone Deacetylase and Bromodomain Inhibition in Non-Small Cell Lung Cancer. Cancer Discov 2017;7(8):852–67 doi 10.1158/2159-8290.CD-16-1020. [PubMed: 28408401]
15. Kim K, Skora AD, Li Z, Liu Q, Tam AJ, Blosser RL, et al. Eradication of metastatic mouse cancers resistant to immune checkpoint blockade by suppression of myeloid-derived cells. Proc Natl Acad Sci U S A 2014;111(32):11774–9 doi 10.1073/pnas.1410626111. [PubMed: 25071169]
16. Peng D, Kryczek I, Nagarsheth N, Zhao L, Wei S, Wang W, et al. Epigenetic silencing of TH1-type chemokines shapes tumour immunity and immunotherapy. Nature 2015;527(7577):249–53 doi 10.1038/nature15520. [PubMed: 26503055]
17. Sheng W, LaFleur MW, Nguyen TH, Chen S, Chakravarthy A, Conway JR, et al. LSD1 Ablation Stimulates Anti-tumor Immunity and Enables Checkpoint Blockade. Cell 2018;174(3):549–63 e19 doi 10.1016/j.cell.2018.05.052. [PubMed: 29937226]
18. Manguso RT, Pope HW, Zimmer MD, Brown FD, Yates KB, Miller BC, et al. In vivo CRISPR screening identifies Ptpn2 as a cancer immunotherapy target. Nature 2017;547(7664):413–8 doi 10.1038/nature23270. [PubMed: 28723893]

19. Pan D, Kobayashi A, Jiang P, Ferrari de Andrade L, Tay RE, Luoma AM, et al. A major chromatin regulator determines resistance of tumor cells to T cell-mediated killing. Science 2018;359(6377): 770–5 doi 10.1126/science.aao1710. [PubMed: 29301958]
20. Patel SJ, Sanjana NE, Kishton RJ, Eidizadeh A, Vodnala SK, Cam M, et al. Identification of essential genes for cancer immunotherapy. Nature 2017;548(7669):537–42 doi 10.1038/nature23477. [PubMed: 28783722]
21. Chen S, Sanjana NE, Zheng K, Shalem O, Lee K, Shi X, et al. Genome-wide CRISPR screen in a mouse model of tumor growth and metastasis. Cell 2015;160(6):1246–60 doi 10.1016/j.cell.2015.02.038. [PubMed: 25748654]
22. De Koning L, Corpet A, Haber JE, Almouzni G. Histone chaperones: an escort network regulating histone traffic. Nat Struct Mol Biol 2007;14(11):997–1007 doi 10.1038/nsmb1318. [PubMed: 17984962]
23. Gao Y, Gan H, Lou Z, Zhang Z. Asf1a resolves bivalent chromatin domains for the induction of lineage-specific genes during mouse embryonic stem cell differentiation. Proc Natl Acad Sci U S A 2018;115(27):E6162–E71 doi 10.1073/pnas.1801909115. [PubMed: 29915027]
24. Peng W, Chen JQ, Liu C, Malu S, Creasy C, Tetzlaff MT, et al. Loss of PTEN Promotes Resistance to T Cell-Mediated Immunotherapy. Cancer Discov 2016;6(2):202–16 doi 10.1158/2159-8290.CD-15-0283. [PubMed: 26645196]
25. Zhu H, Bengsch F, Svoronos N, Rutkowski MR, Bitler BG, Allegrezza MJ, et al. BET Bromodomain Inhibition Promotes Anti-tumor Immunity by Suppressing PD-L1 Expression. Cell Rep 2016;16(11):2829–37 doi 10.1016/j.celrep.2016.08.032. [PubMed: 27626654]
26. Spranger S, Bao R, Gajewski TF. Melanoma-intrinsic beta-catenin signalling prevents anti-tumour immunity. Nature 2015;523(7559):231–5 doi 10.1038/nature14404. [PubMed: 25970248]
27. Ebert PJR, Cheung J, Yang Y, McNamara E, Hong R, Moskalenko M, et al. MAP Kinase Inhibition Promotes T Cell and Anti-tumor Activity in Combination with PD-L1 Checkpoint Blockade. Immunity 2016;44(3):609–21 doi 10.1016/j.immuni.2016.01.024. [PubMed: 26944201]
28. Wu Y, Li X, Yu J, Bjorkholm M, Xu D. ASF1a inhibition induces p53-dependent growth arrest and senescence of cancer cells. Cell Death Dis 2019;10(2):76 doi 10.1038/s41419-019-1357-z. [PubMed: 30692519]
29. Mills CD. Anatomy of a discovery: m1 and m2 macrophages. Front Immunol 2015;6:212 doi 10.3389/fimmu.2015.00212. [PubMed: 25999950]
30. Wang W, Marinis JM, Beal AM, Savadkar S, Wu Y, Khan M, et al. RIP1 Kinase Drives Macrophage-Mediated Adaptive Immune Tolerance in Pancreatic Cancer. Cancer Cell 2018;34(5): 757–74 e7 doi 10.1016/j.ccell.2018.10.006. [PubMed: 30423296]
31. Fleetwood AJ, Lawrence T, Hamilton JA, Cook AD. Granulocyte-macrophage colony-stimulating factor (CSF) and macrophage CSF-dependent macrophage phenotypes display differences in cytokine profiles and transcription factor activities: implications for CSF blockade in inflammation. J Immunol 2007;178(8):5245–52 doi 10.4049/jimmunol.178.8.5245. [PubMed: 17404308]
32. Verreck FA, de Boer T, Langenberg DM, Hoeve MA, Kramer M, Vaisberg E, et al. Human IL-23-producing type 1 macrophages promote but IL-10-producing type 2 macrophages subvert immunity to (myco)bacteria. Proc Natl Acad Sci U S A 2004;101(13):4560–5 doi 10.1073/pnas.0400983101. [PubMed: 15070757]
33. Lai WKM, Pugh BF. Understanding nucleosome dynamics and their links to gene expression and DNA replication. Nat Rev Mol Cell Biol 2017;18(9):548–62 doi 10.1038/nrm.2017.47. [PubMed: 28537572]
34. Pchelintsev NA, McBryan T, Rai TS, van Tuyn J, Ray-Gallet D, Almouzni G, et al. Placing the HIRA histone chaperone complex in the chromatin landscape. Cell Rep 2013;3(4):1012–9 doi 10.1016/j.celrep.2013.03.026. [PubMed: 23602572]
35. Shalek AK, Satija R, Adiconis X, Gertner RS, Gaublomme JT, Raychowdhury R, et al. Single-cell transcriptomics reveals bimodality in expression and splicing in immune cells. Nature 2013;498(7453):236–40 doi 10.1038/nature12172nature12172 [pii]. [PubMed: 23685454]

36. Wills QF, Livak KJ, Tipping AJ, Enver T, Goldson AJ, Sexton DW, et al. Single-cell gene expression analysis reveals genetic associations masked in whole-tissue experiments. Nat Biotechnol 2013;31(8):748–52 doi 10.1038/nbt.2642nbt.2642 [pii]. [PubMed: 23873083]
37. Gubin MM, Esaulova E, Ward JP, Malkova ON, Runci D, Wong P, et al. High-Dimensional Analysis Delineates Myeloid and Lymphoid Compartment Remodeling during Successful Immune-Checkpoint Cancer Therapy. Cell 2018;175(4):1014–30 e19 doi 10.1016/j.cell.2018.09.030. [PubMed: 30343900]
38. Gasco S, Zaragoza P, Garcia-Redondo A, Calvo AC, Osta R. Inflammatory and non-inflammatory monocytes as novel prognostic biomarkers of survival in SOD1G93A mouse model of Amyotrophic Lateral Sclerosis. PLoS One 2017;12(9):e0184626 doi 10.1371/journal.pone.0184626. [PubMed: 28886177]
39. Yang J, Zhang L, Yu C, Yang XF, Wang H. Monocyte and macrophage differentiation: circulation inflammatory monocyte as biomarker for inflammatory diseases. Biomark Res 2014;2(1):1 doi 10.1186/2050-7771-2-1. [PubMed: 24398220]
40. Li T, Chen ZJ. The cGAS-cGAMP-STING pathway connects DNA damage to inflammation, senescence, and cancer. J Exp Med 2018;215(5):1287–99 doi 10.1084/jem.20180139. [PubMed: 29622565]
41. van de Laar L, Coffer PJ, Woltman AM. Regulation of dendritic cell development by GM-CSF: molecular control and implications for immune homeostasis and therapy. Blood 2012;119(15):3383–93 doi 10.1182/blood-2011-11-370130. [PubMed: 22323450]
42. Lacey DC, Achuthan A, Fleetwood AJ, Dinh H, Roiniotis J, Scholz GM, et al. Defining GM-CSF- and macrophage-CSF-dependent macrophage responses by in vitro models. J Immunol 2012;188(11):5752–65 doi 10.4049/jimmunol.1103426. [PubMed: 22547697]
43. Bayne LJ, Beatty GL, Jhala N, Clark CE, Rhim AD, Stanger BZ, et al. Tumor-derived granulocyte-macrophage colony-stimulating factor regulates myeloid inflammation and T cell immunity in pancreatic cancer. Cancer Cell 2012;21(6):822–35 doi 10.1016/j.ccr.2012.04.025. [PubMed: 22698406]
44. Pylayeva-Gupta Y, Lee KE, Hajdu CH, Miller G, Bar-Sagi D. Oncogenic Kras-induced GM-CSF production promotes the development of pancreatic neoplasia. Cancer Cell 2012;21(6):836–47 doi 10.1016/j.ccr.2012.04.024. [PubMed: 22698407]
45. Lechner MG, Liebertz DJ, Epstein AL. Characterization of cytokine-induced myeloid-derived suppressor cells from normal human peripheral blood mononuclear cells. J Immunol 2010;185(4):2273–84 doi 10.4049/jimmunol.1000901. [PubMed: 20644162]
46. Jung S, Unutmaz D, Wong P, Sano G, De los Santos K, Sparwasser T, et al. In vivo depletion of CD11c+ dendritic cells abrogates priming of CD8+ T cells by exogenous cell-associated antigens. Immunity 2002;17(2):211–20. [PubMed: 12196292]
47. Aktas ON, Ozturk AB, Erman B, Erus S, Tanju S, Dilege S. Role of natural killer cells in lung cancer. J Cancer Res Clin Oncol 2018;144(6):997–1003 doi 10.1007/s00432-018-2635-3. [PubMed: 29616326]
48. Koyama S, Akbay EA, Li YY, Aref AR, Skoulidis F, Herter-Sprie GS, et al. STK11/LKB1 Deficiency Promotes Neutrophil Recruitment and Proinflammatory Cytokine Production to Suppress T-cell Activity in the Lung Tumor Microenvironment. Cancer Res 2016;76(5):999–1008 doi 10.1158/0008-5472.CAN-15-1439. [PubMed: 26833127]
49. Seol JH, Song TY, Oh SE, Jo C, Choi A, Kim B, et al. Identification of small molecules that inhibit the histone chaperone Asf1 and its chromatin function. BMB Rep 2015;48(12):685–90 doi 10.5483/bmbrep.2015.48.12.063. [PubMed: 26058396]
50. Sherr CJ, Beach D, Shapiro GI. Targeting CDK4 and CDK6: From Discovery to Therapy. Cancer Discov 2016;6(4):353–67 doi 10.1158/2159-8290.CD-15-0894. [PubMed: 26658964]
51. Deng J, Wang ES, Jenkins RW, Li S, Dries R, Yates K, et al. CDK4/6 Inhibition Augments Antitumor Immunity by Enhancing T-cell Activation. Cancer Discov 2018;8(2):216–33 doi 10.1158/2159-8290.CD-17-0915. [PubMed: 29101163]
52. Goel S, DeCristo MJ, Watt AC, BrinJones H, Sceneay J, Li BB, et al. CDK4/6 inhibition triggers anti-tumour immunity. Nature 2017;548(7668):471–5 doi 10.1038/nature23465. [PubMed: 28813415]

53. Lizotte PH, Hong RL, Luster TA, Cavanaugh ME, Taus LJ, Wang S, et al. A High-Throughput Immune-Oncology Screen Identifies EGFR Inhibitors as Potent Enhancers of Antigen-Specific Cytotoxic T-lymphocyte Tumor Cell Killing. Cancer Immunol Res 2018;6(12):1511–23 doi 10.1158/2326-6066.CIR-18-0193. [PubMed: 30242021]
54. Love MI, Huber W, Anders S. Moderated estimation of fold change and dispersion for RNA-seq data with DESeq2. Genome Biol 2014;15(12):550 doi 10.1186/s13059-014-0550-8. [PubMed: 25516281]
55. Li W, Xu H, Xiao T, Cong L, Love MI, Zhang F, et al. MAGeCK enables robust identification of essential genes from genome-scale CRISPR/Cas9 knockout screens. Genome Biol 2014;15(12): 554 doi 10.1186/s13059-014-0554-4. [PubMed: 25476604]
56. Yu G, Wang LG, Han Y, He QY. clusterProfiler: an R package for comparing biological themes among gene clusters. OMICS 2012;16(5):284–7 doi 10.1089/omi.2011.0118. [PubMed: 22455463]
57. Rodig N, Ryan T, Allen JA, Pang H, Grabie N, Chernova T, et al. Endothelial expression of PD-L1 and PD-L2 down-regulates CD8+ T cell activation and cytolysis. Eur J Immunol 2003;33(11): 3117–26 doi 10.1002/eji.200324270. [PubMed: 14579280]
58. Chen Z, Cheng K, Walton Z, Wang Y, Ebi H, Shimamura T, et al. A murine lung cancer co-clinical trial identifies genetic modifiers of therapeutic response. Nature 2012;483(7391):613–7 doi 10.1038/nature10937. [PubMed: 22425996]
59. Dobin A, Davis CA, Schlesinger F, Drenkow J, Zaleski C, Jha S, et al. STAR: ultrafast universal RNA-seq aligner. Bioinformatics 2013;29(1):15–21 doi 10.1093/bioinformatics/bts635. [PubMed: 23104886]
60. Anders S, Huber W. Differential expression analysis for sequence count data. Genome Biol 2010;11(10):R106 doi 10.1186/gb-2010-11-10-r106. [PubMed: 20979621]
61. Langmead B, Salzberg SL. Fast gapped-read alignment with Bowtie 2. Nat Methods 2012;9(4): 357–9 doi 10.1038/nmeth.1923. [PubMed: 22388286]
62. Quinlan AR, Hall IM. BEDTools: a flexible suite of utilities for comparing genomic features. Bioinformatics 2010;26(6):841–2 doi 10.1093/bioinformatics/btq033. [PubMed: 20110278]
63. Zhang Y, Liu T, Meyer CA, Eeckhoute J, Johnson DS, Bernstein BE, et al. Model-based analysis of ChIP-Seq (MACS). Genome Biol 2008;9(9):R137 doi 10.1186/gb-2008-9-9-r137. [PubMed: 18798982]
64. Yu G, Wang LG, He QY. ChIPseeker: an R/Bioconductor package for ChIP peak annotation, comparison and visualization. Bioinformatics 2015;31(14):2382–3 doi 10.1093/bioinformatics/btv145. [PubMed: 25765347]
65. Heinz S, Benner C, Spann N, Bertolino E, Lin YC, Laslo P, et al. Simple combinations of lineage-determining transcription factors prime cis-regulatory elements required for macrophage and B cell identities. Mol Cell 2010;38(4):576–89 doi 10.1016/j.molcel.2010.05.004. [PubMed: 20513432]
66. Misharin AV, Morales-Nebreda L, Mutlu GM, Budinger GR, Perlman H. Flow cytometric analysis of macrophages and dendritic cell subsets in the mouse lung. Am J Respir Cell Mol Biol 2013;49(4):503–10 doi 10.1165/rcmb.2013-0086MA. [PubMed: 23672262]
67. Zheng GX, Terry JM, Belgrader P, Ryvkin P, Bent ZW, Wilson R, et al. Massively parallel digital transcriptional profiling of single cells. Nat Commun 2017;8:14049 doi 10.1038/ncomms14049. [PubMed: 28091601]
68. Jenkins RW, Aref AR, Lizotte PH, Ivanova E, Stinson S, Zhou CW, et al. Ex Vivo Profiling of PD-1 Blockade Using Organotypic Tumor Spheroids. Cancer Discov 2018;8(2):196–215 doi 10.1158/2159-8290.CD-17-0833. [PubMed: 29101162]

## SIGNIFICANCE

Using an *in vivo* epigenetic CRISPR screen, we identified *Asf1a* as a critical regulator of lung ADC sensitivity to anti-PD-1 therapy. *Asf1a* deficiency synergized with anti-PD-1 immunotherapy by promoting M1-like macrophage polarization and T cell activation. Thus, we provide a new immunotherapeutic strategy for this subtype of lung ADC patients.

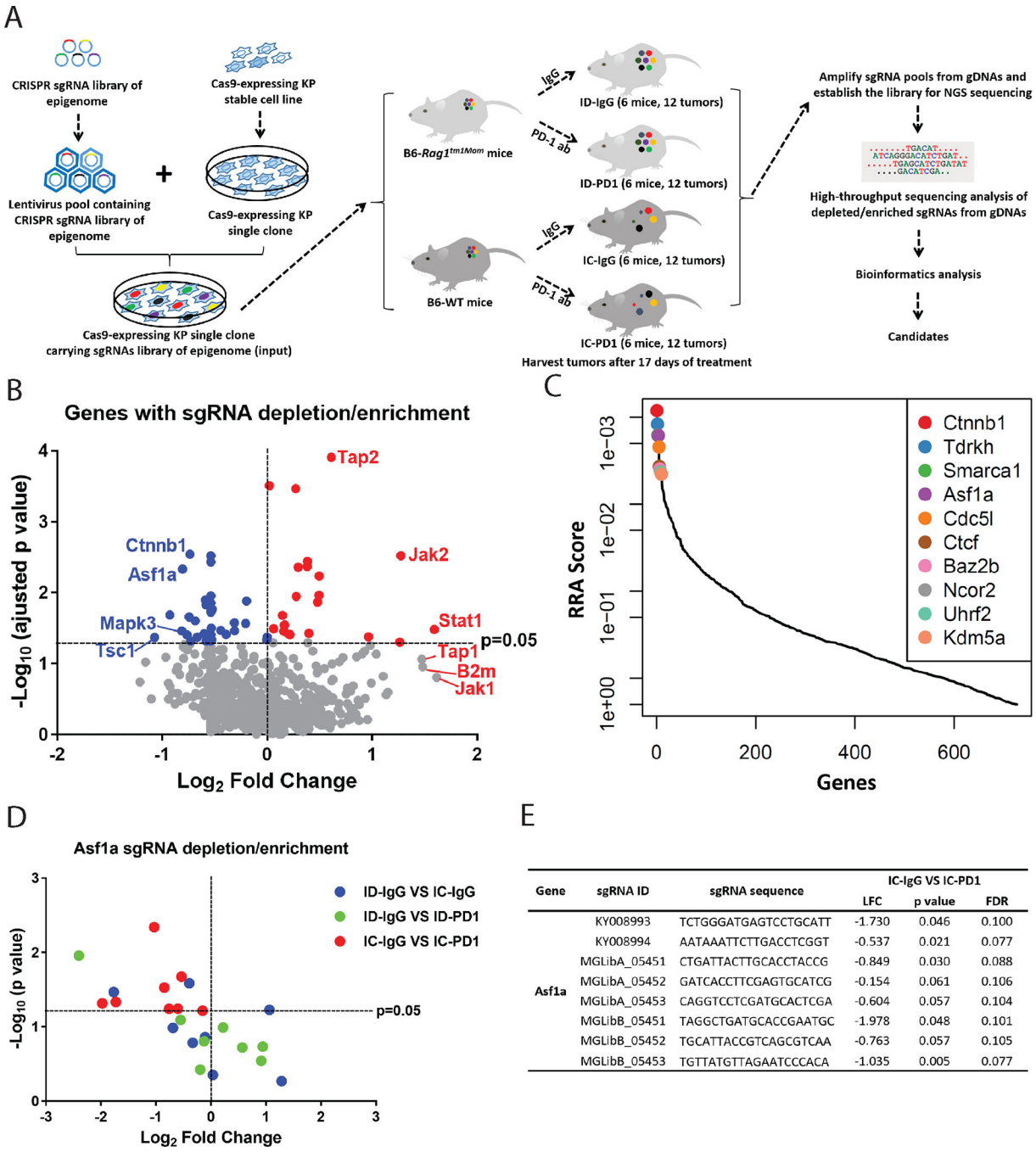


| Gene | sgRNA ID | sgRNA sequence | IC-IgG VS IC-PD1 | | |
|---|---|---|---|---|---|
| | | | LFC | p value | FDR |
| Asf1a | KY008993 | TCTGGGATGAGTCCTGCATT | -1.730 | 0.046 | 0.100 |
| | KY008994 | AATAAATTCTTGACCTCGGT | -0.537 | 0.021 | 0.077 |
| | MGLibA_05451 | CTGATTACTTGCACCTACCG | -0.849 | 0.030 | 0.088 |
| | MGLibA_05452 | GATCACCTTCGAGTGCATCG | -0.154 | 0.061 | 0.106 |
| | MGLibA_05453 | CAGGTCCTCGATGCACTCGA | -0.604 | 0.057 | 0.104 |
| | MGLibB_05451 | TAGGCTGATGCACCGAATGC | -1.978 | 0.048 | 0.101 |
| | MGLibB_05452 | TGCATTACCGTCAGCGTCAA | -0.763 | 0.057 | 0.105 |
| | MGLibB_05453 | TGTTATGTTAGAATCCCACA | -1.035 | 0.005 | 0.077 |

**Figure 1. *In vivo* epigenome-wide CRISPR screen identifies *Asf1a* as a negative regulator of response to anti-PD-1 therapy.**

**A**, Strategy of *in vivo* epigenome-wide CRISPR screen. 12 tumors from 6 mice were included in each group of the screen. **B**, Volcano plot illustrating the comparison of IC-IgG and IC-PD1 genes whose knockout (KO) can enhance (blue) or inhibit (red) sensitivity to anti-PD-1 treatment. Some top candidates are highlighted, along with positive control genes whose KO is expected to enhance or inhibit anti-PD-1 treatment. **C**, Illustration of the top 10 candidates from (**B**). **D**, Scatter plot showing the performance of 8 *Asf1a* sgRNAs in the

comparisons indicated “ID-IgG VS IC-IgG”, “ID-IgG VS ID-PD1” and “IC-IgG VS IC-PD1”. **E**, Detailed information on the performance of 8 *Asf1a* sgRNAs in the comparison “IC-IgG VS IC-PD1”. ID, immunodeficient B6 *Rag1*−/− mice; IC, immunocompetent B6 mice; IgG, IgG treatment; PD1, anti-PD-1 treatment.

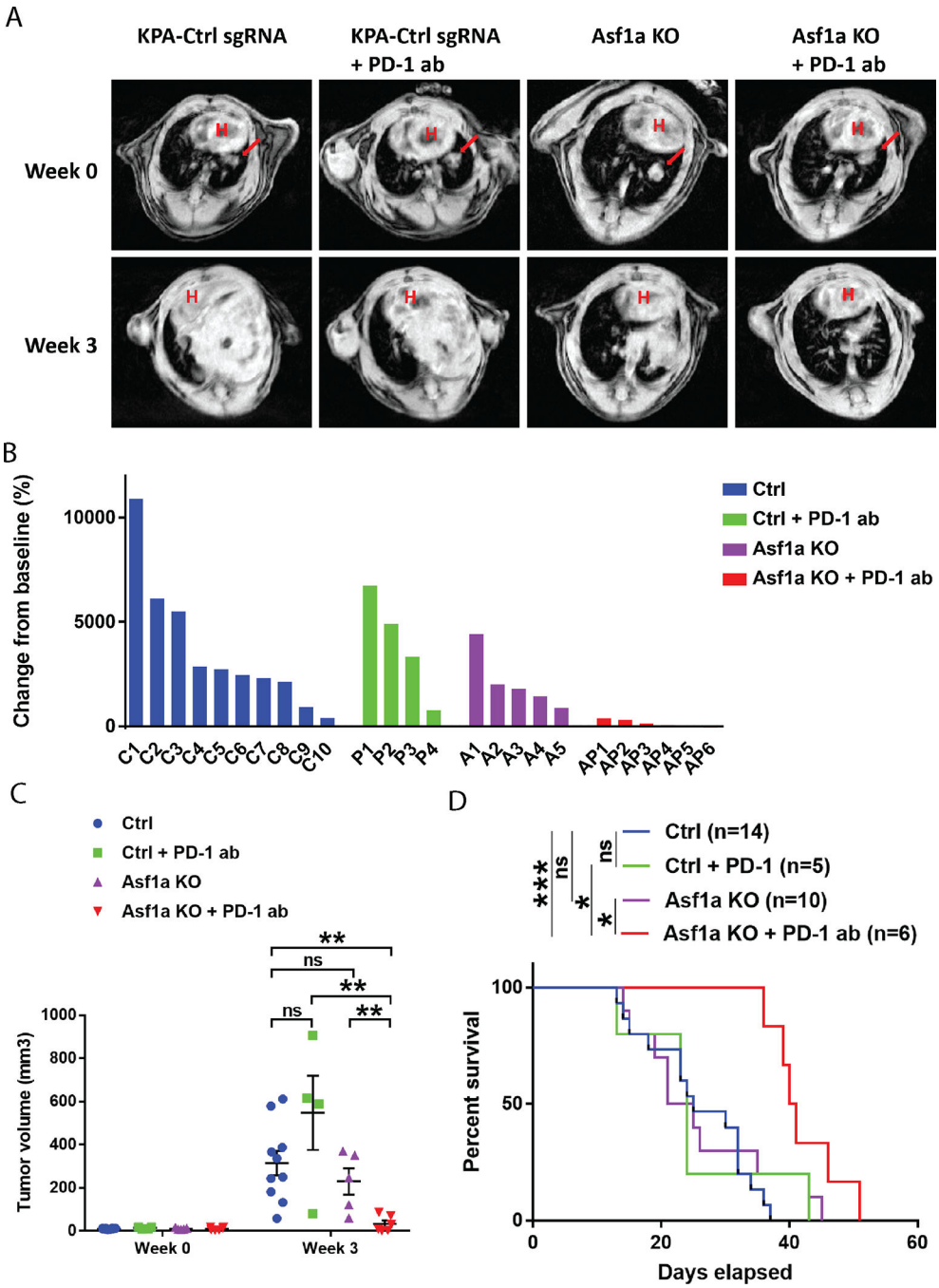


**Figure 2. *Asf1a* deficiency synergizes with anti-PD-1 treatment to inhibit tumor progression.**

**A**, Representative MRI scans (1 of 24 scanned images of each mouse) showing mouse lung tumors before and after treatment. The red arrow indicates the single tumor nodule on the left lobe. “H” indicates the heart. **B**, Waterfall plot showing percentages changes in tumor volume in response to treatment. Each column represents one mouse. **C**, Dot plot illustrating the tumor volume across the different treatment groups. (Ctrl, n=10; Ctrl + PD-1 ab, n=4; Asf1a KO, n=5; Asf1a KO + PD-1 ab, n=6). 4 mice in Ctrl group, 1 mouse in Ctrl + PD-1 ab group, and 5 mice in Asf1a KO group died prior to week 3 MRI imaging, and hence are

excluded here. **D**, Survival curve for each group in the treatment study. (Ctrl, n=14; Ctrl + PD-1 ab, n=5; Asf1a KO, n=10; Asf1a KO + PD-1 ab, n=6). All data are mean ± SEM. *$p$ < 0.05, **$p$ < 0.01, *** $p$ <0.001

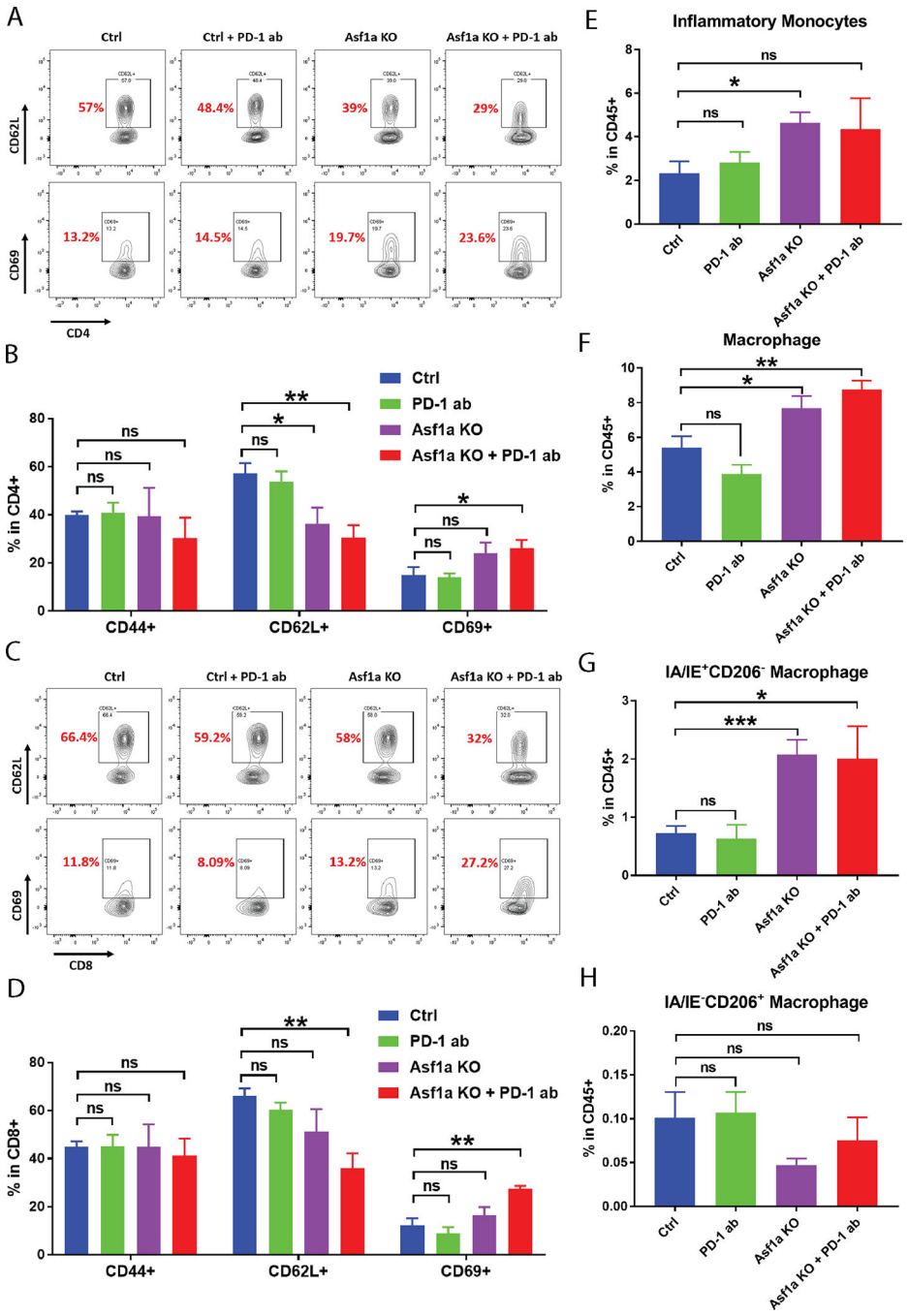


**Figure 3. *Asf1a* deficiency and anti-PD-1 treatment promotes T cell activation, inflammatory response and M1-like macrophage polarization.**

**A**, Representative flow cytometry analysis of $CD62L^+$ (naive T cell marker) and $CD69^+$ (T cell activation marker) populations of $CD4^+$ T cells across all treatment groups. **B**, Bar graphs comparing the expression of $CD44^+$ (T cell activation marker), $CD62L^+$ and $CD69^+$ populations of $CD4^+$ T cells across all treatment groups. **C**, Representative flow cytometry analysis of $CD62L^+$ and $CD69^+$ populations of $CD8^+$ T cells. **D**, Bar graph comparing the expression of $CD44^+$, $CD62L^+$ and $CD69^+$ populations of $CD8^+$ T cells. **E–H**, Flow

cytometry analysis on changes in the expression of inflammatory monocytes ($CD11b^+/Gr1^-/SelecF^-/Ly6c^+$) (**E**), macrophages ($CD11b^+/Gr1^-/F4/80^+$) (**F**), M1-like macrophages ($CD11b^+/Gr1^-/F4/80^+/MHC\text{-}II^+/CD206^-$) (**G**), and M2-like macrophages ($CD11b^+/Gr1^-/F4/80^+/MHC\text{-}II^-/CD206^+$) (**H**) in $CD45^+$ cells. For all flow cytometry experiments, the whole tumor-bearing lungs from an IV injection model were harvested and processed after 1 week of treatment. (Ctrl, n=5; PD-1 ab, n=5; Asf1a KO, n=5; Asf1a KO + PD-1 ab, n=5). All data are mean ± SEM. $*p < 0.05$, $**p < 0.01$, $***p < 0.001$

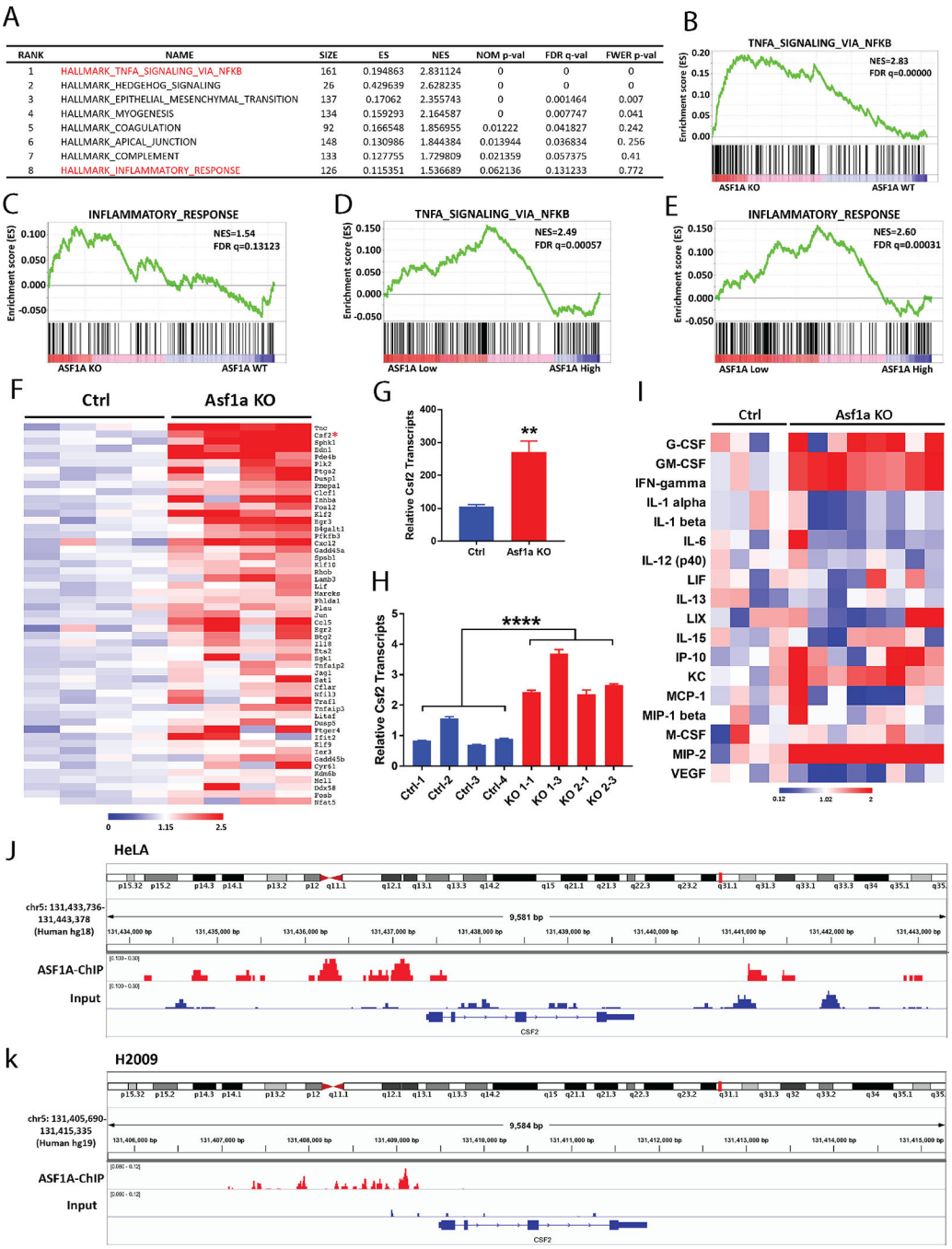


**Figure 4. *Asf1a* deficiency activates TNFA signaling and upregulating GM-CSF.**

**A**, Gene set enrichment analysis (GSEA) showing the top 8 enriched pathways in KP cells with *Asf1a* KO. **B**, Enrichment of genes associated with TNFA_SIGNALING_VIA_NFKB in KP cells with *Asf1a* KO. **C**, Enrichment of genes associated with INFLAMMATORY_RESPONSE in KP cells with *Asf1a* KO. **D**, Enrichment of genes associated with TNFA_SIGNALING_VIA_NFKB in human lung ADC tumors with low *ASF1A* expression. **E**, Enrichment of genes associated with INFLAMMATORY_RESPONSE in human lung ADC tumors with low *ASF1A* expression.

Top 25% and bottom 25% of ASF1A expression levels were determined using RNA-seq data. **F**, Heatmap of the genes that comprise the TNFA_SIGNALING_VIA_NFKB gene set in KP cells with or without *Asf1a* KO. Red star marks the *Csf2* gene. **G**, Relative *Csf2* transcripts in KP cells with or without *Asf1a* KO from RNA-seq data. **H,** Expression of *Csf2* in KP cells with or without *Asf1a* KO as determined by real-time qPCR. **I**, Luminex analyses of chemokines/cytokines secreted in cell culture medium harvested 30 hours after the cells were seeded. **J**, ChIP-seq data of HeLa cells showing that ASF1A occupies the *CSF2* promoter. **K**, ChIP-seq data of H2009 cells showing that ASF1A occupies the *CSF2* promoter. Genomic DNA from H2009 cells was used as input control. All data are mean ± SEM. $^{**}p < 0.01$, $^{****}p < 0.0001$

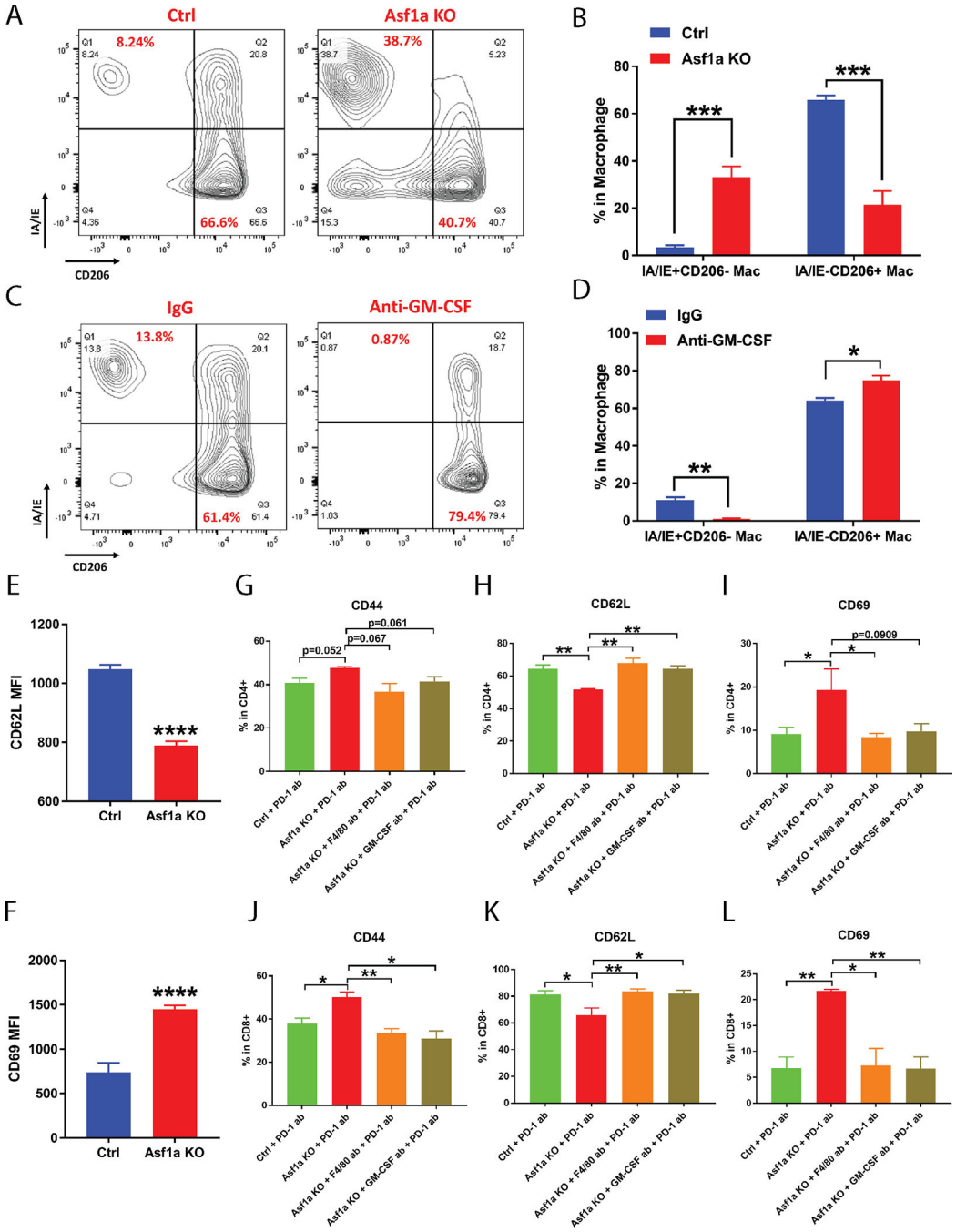


**Figure 5. *Asf1a* deficiency promotes M1-like macrophage polarization and T cell activation through upregulation of GM-CSF.**

**A**, Flow cytometry analysis of IA/IE and CD206 expression in macrophages co-cultured with KP-Ctrl cells or KP-*Asf1a* KO cells for 7 days. **B**, Bar graph showing the percentages of IA/IE$^{+}$CD206$^{-}$ (M1-like) macrophages and IA/IE$^{-}$CD206$^{+}$ (M2-like) macrophages from the co-culture experiment shown in (**A**). (Ctrl, n=4; Asf1a KO, n=6). **C**, Flow cytometry analysis of IA/IE and CD206 expression in macrophages co-cultured with KP cells in the presence of IgG or anti-GM-CSF for 7 days. **D**, Bar graph showing the percentages of IA/IE

$^{+}$CD206$^{-}$ (M1-like) macrophages and IA/IE$^{-}$CD206$^{+}$ (M2-like) macrophages from the co-culture experiment shown in (**C**). (IgG, n=3; Anti-GM-CSF, n=3). **E-F**, Flow cytometry analysis of changes in expression of CD62L (**E**), CD69 (**F**) in OT-I T cells co-cultured with macrophages which were sorted from the co-culture system shown in (**A**). (Ctrl, n=3; Asf1a KO, n=7). **G-I**, Flow analysis of the expression of CD44$^{+}$(**G**), CD62L$^{+}$(**H**) and CD69$^{+}$(**I**) populations in CD4$^{+}$ T cells. **J-L**, Flow analysis of the expression of CD44$^{+}$ (**J**), CD62L$^{+}$ (**K**) and CD69$^{+}$ (**L**) populations in CD8$^{+}$ T cells. For flow cytometry analyses in (**G-L**), whole tumor-bearing lungs from the trans-thoracic injection model were harvested and processed for flow cytometry analysis after 3 weeks of treatment. (Ctrl + PD-1 ab, n=4; Asf1a KO + PD-1 ab, n=4; Asf1a KO + F4/80 ab + PD-1 ab, n=5; Asf1a KO + GM-CSF ab + PD-1, n=4). All data are mean ± SEM. *$p < 0.05$, **$p < 0.01$, ***$p < 0.001$, **** $p < 0.0001$ (MFI, mean fluorescence intensity).

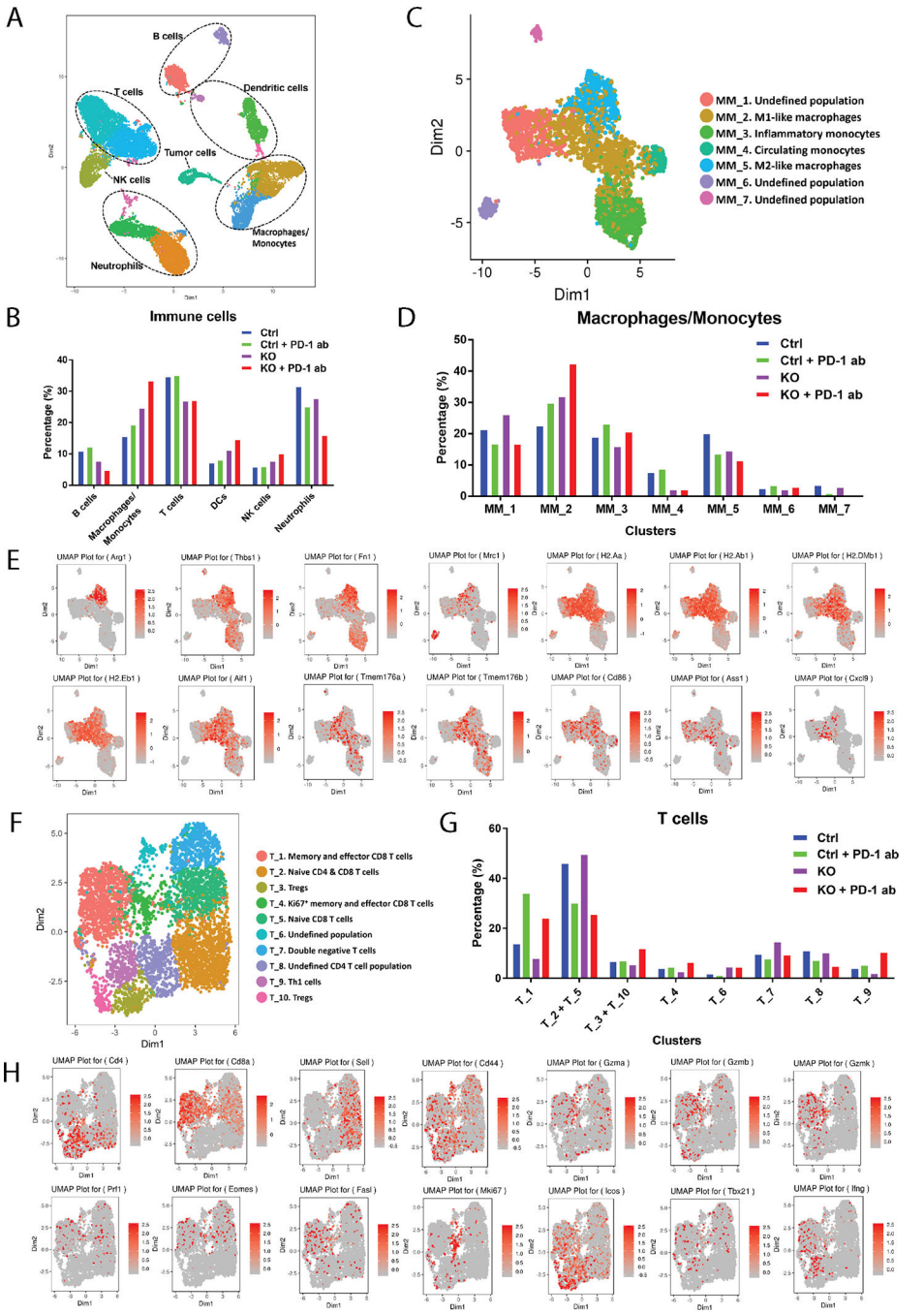


**Figure 6. Single-cell analyses of intratumoral immune cell populations confirm the alterations of macrophage and T cell populations.**

**A**, Umap plot showing clusters of tumor cells (center) and intratumoral immune cell populations. **B**, Changes in the different immune compartments in response to indicated treatments. **C**, Umap plot showing secondary clusters of macrophages/monocytes. **D**, Changes in different macrophage/monocyte subpopulations in response to indicated treatments. **E**, Umap plots show the expression of M2 macrophage marker genes (*Arg1*, *Thbs1*, *Fn1* and *Mrc1*) and M1 macrophage marker genes (*H2.Aa*, *H2.Ab1*, *H2.DMb1*,

*H2.Eb1*, *Aif1*, *Tmem176a*, *Tmem176b*, *Cd86*, *Ass1* and *Cxcl9*) in the macrophage/monocyte subpopulations. **F**, Umap plot showing secondary clusters of T cell population. **G**, Changes in different T cell subpopulations in response to indicated treatments. **H**, Umap plots showing the expression of T cell marker genes (*Cd4*, *Cd8*, *Sell*, *Cd44*, *Gzma*, *Gzmb*, *Gzmk*, *Prf1*, *Eomes*, *FasI*, *Mki67*, *Icos*, *Tbx21* and *Ifng*) in T cell subpopulations.

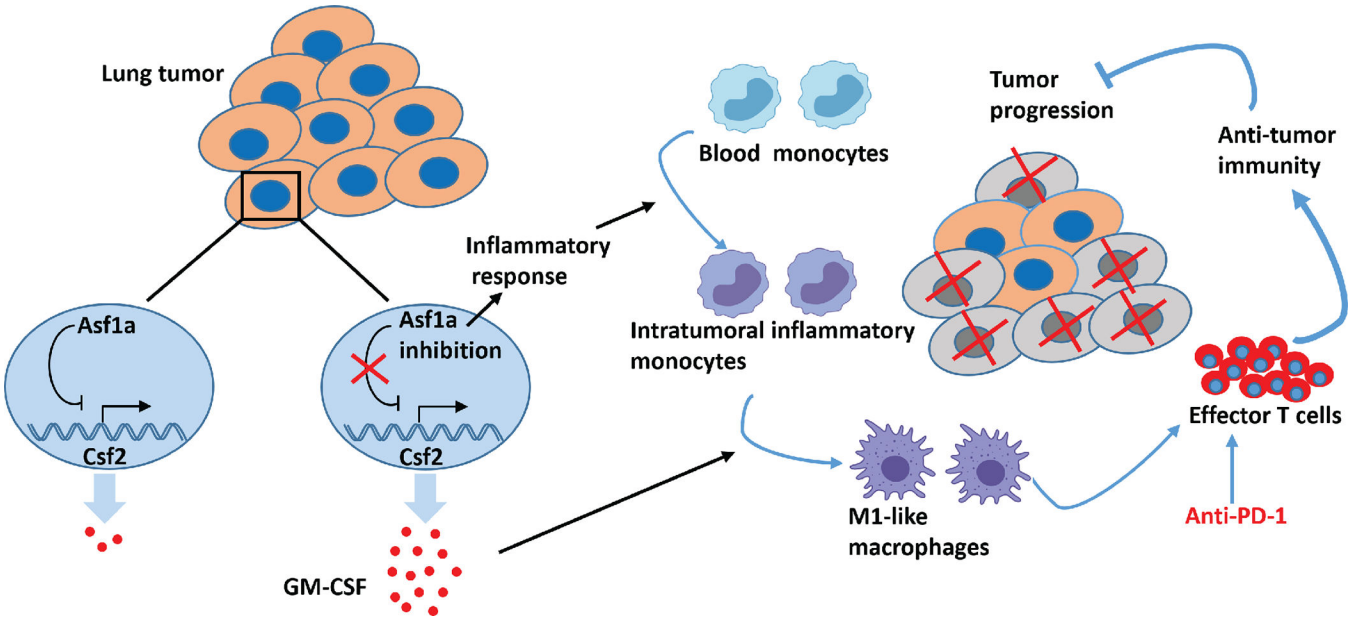


**Figure 7. Working model for *Asf1a* deficiency combined with anti-PD-1 combination therapy.**

Tumor cell-intrinsic *Asf1a* deficiency promotes an inflammatory response and GM-CSF secretion, which promotes M1-like macrophage polarization and T cell activation. Anti-PD-1 therapy also promotes T cell activation. Thus, *Asf1a* KO synergizes with anti-PD-1 treatment to promote anti-tumor immunity.